University of Copenhagen
Master's Thesis in Physics

Deterministic Fourier Microscopy

Rasmus Buus Nielsen KU-ID: fbg450

1 Preface

The content covered in this thesis has been limited to the core theories and methods necessary to address the broad topic of ptychography, it is as such recommended that the reader has knowledge of electromagnetism, optics, differential equations and Fourier transformations. The appendix provides further background theory to which the author has not directly contributed. The appendix concludes with the theory on the use of tilt aberration for phase reconstruction, which sets the starting point of this project. It is assumed throughout that the experimental parameters are known exactly and only the determination of sample properties is of interest. The effect of uncertainty in the experimental parameters will be discussed at the end.

2 Abstract

Fourier Ptychography calculates sample transmission and optical phase differences using an iterative error reduction pipeline together with efficient methods for simulating light propagation.[1] The method relies on an initial guess for transmission and optical phase differences, and this non-deterministic guess must contain approximations or random elements for unknown parts. This project focuses on the exploration and development of Deterministic Fourier Ptychography as a new method for providing fast, high resolution reconstructions of optical phase differences. The new approach deterministically calculates the phase in the detector plane by introducing a Gaussian apodizer in a Fourier Ptychographic Microscopy setup. This is then combined with the stitching used in Fourier Ptychography to reach a deterministic solution in the sample plane. My novel contribution is the use of algebra to show that a result can be achieved using feasible approximations instead of an iterative process relying on a guess. The stitching inherited from Fourier Ptychography is made non-iterative to allow for this new step. The approach would carry over the advantages of high field of view and high resolution from Fourier Ptychography while reducing computation time. The initial work on the new deterministic method shows that it could potentially be much quicker to calculate and be completely independent of any starting guess as previously used.

Contents

3 Introduction & Background

Typical microscopes have a trade-off between numerical aperture (NA) and Field of View (FOV).[2] An imaging system with high NA captures many diffracted rays from each point on a small area of the sample, while one with a high FOV captures a few diffracted rays from each point on a large area of the sample. The combination of high NA and high FOV requires a lens where each position on the lens correctly focuses rays from many different angles. It also requires a detector which can capture this information on the scale of billions of pixels (gigapixels). This is expensive if not impossible in most cases. Fourier Ptychography offers an alternative by combining many images with a high FOV to create an image with an artificially high NA. To do this the images are simulated backwards through the imaging system to restore the state of the wavefield before the objective. Here they are combined into one wavefield with contributions from diffraction to many angles thus practically increasing the NA. This reconstruction of the wavefield also makes it possible to image optical phase differences from variations in the length of the optical path through the sample.

Fourier Ptychography is especially useful for biological and medical imaging where the combination of phase contrast, high FOV and high resolution allows for observation of spatially rare phenomena and the context of these phenomena.[18] Figure 1 shows an example with an image of cell clusters where subcellular phenomenon can be observed, it also shows that the initial guess makes a difference.[3] The method is now used in a wide variety of different setups from portable, high resolution microscopes using consumer grade lenses[4,5] to X-ray imaging at a synchrotron using lens translation.[6,7]

Deterministic Fourier Ptychography has the possibility to be a novel improvement to Fourier Ptychography. It has many of the advantages while eliminating the need for a starting guess and potentially decreasing the computation time. The method is computationally complex and the conversion from continuous wavefields to discrete data requires thorough consideration to avoid unnecessary loss of information. The focus on the development of the method means that the theory and accuracy of the methods are explored while computational performance is neglected as long as it doesn't hinder usefulness. This might seem contrary to the possibility of reducing the computation time of Fourier Ptychography but it first has to be established if the new method can produce results similar to or better than Fourier Ptychography.

First follows a brief introduction to the concept of optical phase and phase contrast imaging. Then

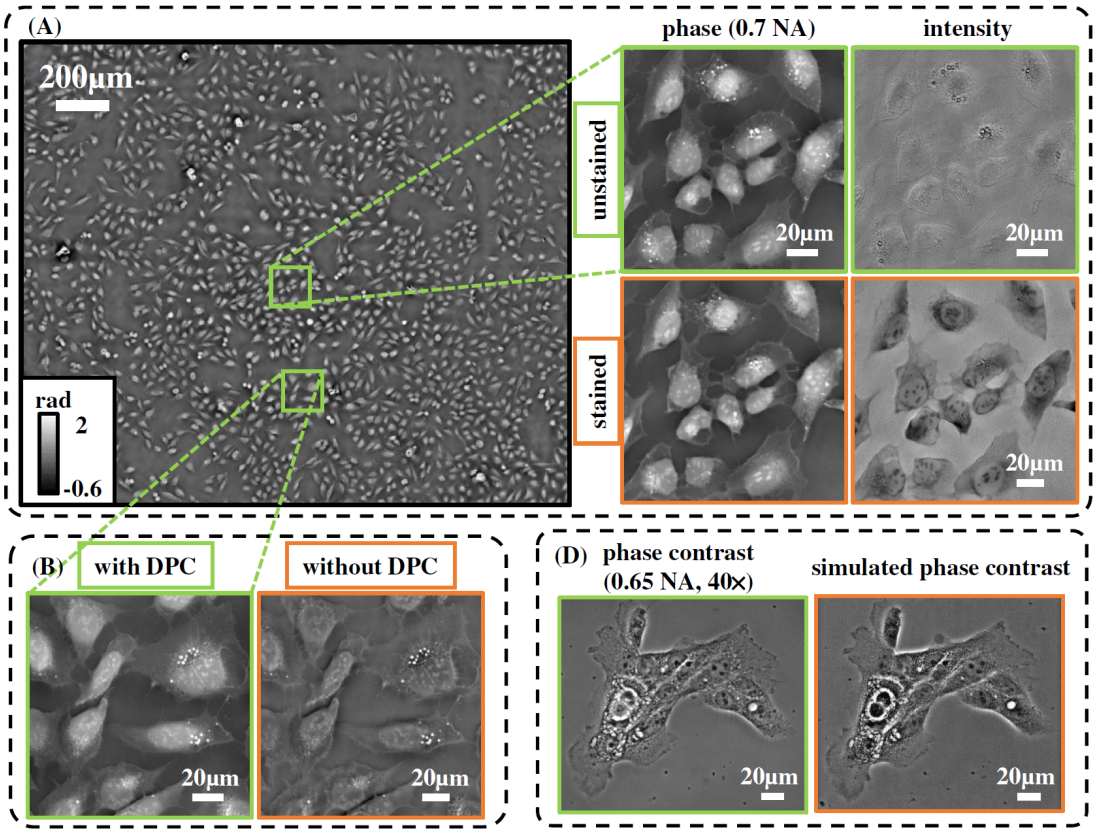

Figure 1: Image from "Computational illumination for high-speed in vitro Fourier Ptychographic microscopy" [3]. A) Fourier Ptychographic phase reconstruction from a 4x 0.2 NA objective resulting in an image with an artificial NA of 0.7. Zoom-in to the right shows that phase can be used without staining the sample. B) Comparing Phase reconstruction when using an initial guess derived from Differential Phase Contrast (DPC). D) phase contrast image from a 40x 0.65 NA objective compared with a forward simulated image from the reconstruction.

follows the introduction to Fourier Ptychography and lens translation imaging which makes it possible to use Fourier Ptychography in different experimental setups. Next, it is shown how correction of lens aberrations can be included in Fourier Ptychography. Then Differential Phase Contrast is presented as an independent method for doing deterministic phase contrast imaging. Finally, it is shown how Fourier Ring Correlation can be used to quantitatively determine the level of detail in the result.

3.1 Phase Contrast Imaging

The phase of a wave isn't directly measurable but phase contrast methods can be used to calculate phase differences between locations on a sample. Imaging using wavefield phase differences allows contrast between materials with identical elements but differing refraction. This is especially useful for imaging biological and medical samples as these contain very similar elemental composition across the sample while having varying refraction. It is possible to image such samples without phase contrast imaging by introducing a fluorescent compound which binds to specific parts of the sample but this has other disadvantages. For X-rays with energies above approx. 5 keV the real part of the refractive index which governs refraction is always higher than the imaginary part which governs absorption.[8] This means that even for a sample consisting of a single material with varying thickness the changes in phase could allow for higher contrast than the changes in absorption.
To understand phase contrast imaging it is necessary to understand that the wave nature of light means that it has a repeating phase. The phase of the wave in a certain location is whether the wave is at a crest, through or in-between, see figure 2. It is intuitive that the phase is repeating so the phase doesn't tell how far the location is from the source. The phase is however dependent on the properties of the electromagnetic wave and it depends on what the wave has interacted with. The optical path length of a wave changes when the measured sample has a refraction index different from air. It is exactly these changes that can be used to restore information about the sample.

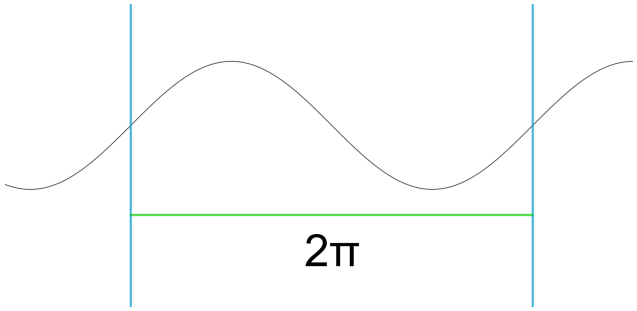

Figure 2

To determine the sample properties the wavelength of the wave must be known as waves with different wavelengths, λ, will diffract to different angles, θ, for a given phase differential:[8]

$$\theta = \frac{\lambda}{2\pi} \nabla_{\perp} \phi \tag{1}$$

The wave must be approximated as monochromatic as contributions from different wavelengths can't be separated. In reality light can't be perfectly monochromatic so the requirement is that the temporal coherence must be high enough for the phase to be well defined through the entire optical setup. For the angle to be well defined each point on the sample must only be illuminated from a single angle as each incident angle has a different exit angle. This means the source must be assumed to be a point and the distance to the sample should be large enough for the phase to be constant across the sample. Again, the perfect case isn't possible but the spatial coherence must be high enough to assume that the entire sample is illuminated from the same angle. Together the requirement of temporal coherence and spatial coherence means that the illumination must be coherent. This is easy to achieve for visible light as LEDs can be assumed to be coherent. It is much harder to achieve coherent illumination in the X-ray regime and it puts constraints on which experimental setups are possible. For coherent X-rays it is practically impossible to change the illumination angle and it is thus necessary to change Fourier Ptychography to account for this. [9]

3.2 Fourier Ptychography

Fourier Ptychography is here presented as a previous method for phase retrieval to provide background for the development of Deterministic Fourier Ptychography. Fourier Ptychography is also used for comparing performance.

Normally the resolving power of an imaging system is limited by the Abbe diffraction limit:

$$d = \frac{\lambda}{2NA} \tag{2}$$

$$NA = n\sin(\theta) \tag{3}$$

The numerical aperture (NA) is a property of the objective lens and describes to which limit the lens can capture diffracting rays. It is impossible to increase NA beyond the refraction coefficient, n, as long as materials have positive refraction coefficients. [13,14] This is since waves must have an imaginary wavenumber in the direction of propagation in order to contain information on details smaller than $\frac{\lambda}{2n}$. waves with imaginary wavenumbers disappear over short distances as evanescent waves. Discussion of materials with negative refraction is outside the scope of this project.

The goal of Fourier Ptychography is to reconstruct the wavefield at the sample and artificially increase the numerical aperture by capturing rays diffracted to higher angles. Experimentally this

is done by tilting the incident beam relative to the lens and detector setup and capturing information from diffraction to higher angles than θ.[19] A similar effect can be achieved by translating the lens in the lens plane and detector in the detector plane. Tilting the incident beam causes a translation of the wavefield in the Fourier-plane while lens translation translates the lens function in the Fourier-plane.

The wavefield is only measured at the detector, and only its intensity is measured. Given the optical setup used, it is possible to use theory to describe how the wavefield propagates through the optical elements to finally be measured at the detector.[1] Fourier Ptychography calculates the wavefield at the object by solving the inverse problem of how the detected wavefield is affected by the object.

Propagation of a wavefield determines the amplitude and phase of a known wavefield after it has traveled a distance z. This can be done by applying the Fresnel-Kirchoff integral to the known wavefield, ψ_0, at its initial position. The appendix shows the derivation of the Fresnel-Kirchoff integral, equation 143:

$$\psi_1(x', y') = \frac{-ik \cdot \exp(ikz)}{2\pi z} \int\int \psi_0(x, y) \cdot \exp\left(\frac{ik}{2z} \cdot \left((x - x')^2 + (y - y')^2\right)\right) dxdy \tag{4}$$

The z-axis is the direction of propagation and the wavefield is initially defined in the xy-plane and the resulting wavefield is in the parallel $x'y'$-plane. The appendix shows how the Fresnel-Kirchoff integral is expanded into an equation which can also describe the effects of the imaging system trough aberrations. For applying just the propagation it can be rewritten using the Fourier transform by approximating $x' = \frac{x \cdot k}{2\pi z}$ and $y' = \frac{y \cdot k}{2\pi z}$ inside the integral:

$$\psi_1(x', y') = \frac{-ik \cdot \exp(ikz)}{2\pi z} \exp\left(\frac{ik}{2z} \cdot (x'^2 + y'^2)\right) \cdot \mathscr{F}\left(\exp\left(\frac{ik}{2z} \cdot (x^2 + y^2)\right) \cdot \psi_0(x, y)\right) \tag{5}$$

This approximation makes sense in the Fraunhofer case as it causes the contributions from x' and y' to disappear from the Fourier transform for $z >> \frac{x}{\lambda}$ and $z >> \frac{y}{\lambda}$ respectively.[10] $\mathscr{F}$ is the two-dimensional Fourier transform:

$$\mathscr{F}(\psi_0(x, y)) = \int\int \psi_0(x, y) \cdot \exp(-i \cdot 2\pi \cdot (x \cdot x' + y \cdot y')) \, dxdy \tag{6}$$

Compared to equation 163 this has the advantage that it only contains one Fourier transform as Fourier transforms are the main contribution to computation time for Fourier Ptychography. The experimental setup includes several optical elements which affect the wavefield when it passes through these elements. To account for these effects one or several transfer functions can be applied

to the wavefield. Both Fourier Ptychography and lens translation imaging include a lens and an aperture both of which can be represented as a single combined transfer function. The lens primarily applies a phase change to the wavefield, this phase change depends on the incident position for each part of the wavefield. Assuming a perfectly thin lens then only a phase change is applied:

$$\phi(x, y) = -\frac{k}{2f}(x^2 + y^2) \tag{7}$$

In this case the spatial dependence is such that the thin lens formula can be used to determine when the image of the sample is in focus at the detector:

$$d_2 = \left(\frac{1}{f} - \frac{1}{d_1}\right)^{-1} \tag{8}$$

A sample at a distance of d_1 from the lens is in focus if the detector is at a distance of d_2 on the other side of the lens. Here f is the focal length of the lens.

The aperture simply limits transmission of the wavefield to the area of the plane where the lens is.

A full scan using Fourier Ptychography or lens translation imaging includes many individual measurements. Between measurements the source incident angle is varied for the normal Fourier Ptychography setup. For lens translation imaging the lens and detector are translated in a plane perpendicular to the optical axis. The detector is translated in proportion to the lens translation such that the waves passing through the lens are measured, see figure 3.

For Differential Phase Contrast and Deterministic Fourier Ptychography it matters whether the Fourier Ptychography or the lens translation setup is used. This is since the translation of the lens increases the distance from lens to sample and detector which can cause the sample to be out of focus, similar to the effect of Petzval field curvature. This doesn't matter for the normal Fourier Ptychography method since the Fresnel-Kirchoff integral includes this effect.

The wavefield is of interest in three planes: at the object, before the lens (the Fourier-plane) and at the detector. In lens translation imaging the wavefield in two of these planes is independent of lens translation; The object plane which contains the object to be scanned and the Fourier-plane. For Fourier Ptychography the angle of the source needs to be accounted for. This can be done by multiplying with a position dependent phase which cancels out the angled beams contribution to the gradient of the phase. In both cases the wavefield in the detector plane depends on the lens function and its position or the source angle.

Restoring the wavefield at the sample is done by starting with a guess of the wavefield at the sample,

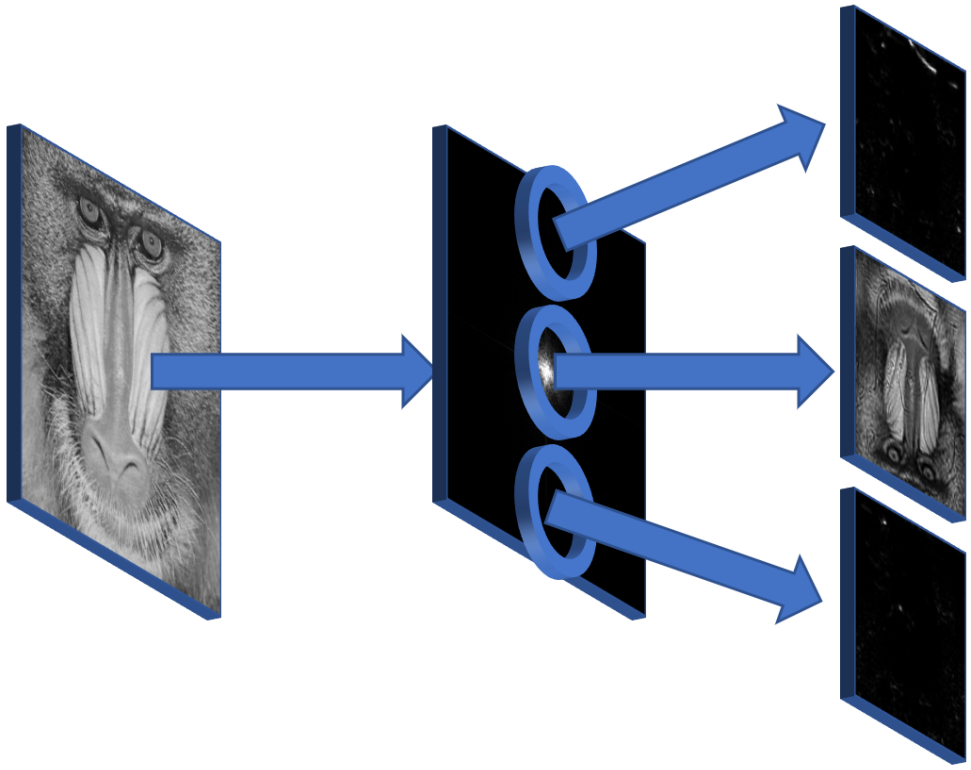

Figure 3: Illustration showing the amplitude of the wavefield in different positions of the optical setup. Not to scale.

this guess can be random, a constant field or determined from another method. This wavefield is then propagated to the Fourier-plane. Here a transfer function, corresponding to the lens position of one of the measured images, is applied to the wavefield.

$$\psi_{out}\left(\vec{r}\right) = T\left(\vec{r}\right) \cdot \psi_{old}^{\mathscr{F}}\left(\vec{r}\right) \tag{9}$$

The superscript $\mathscr{F}$ shows that a wavefield represents the Fourier-plane of the sample. Vector $\vec{r}$ represents the Cartesian spatial coordinates perpendicular to the optical axis:

$$\vec{r} = \begin{bmatrix} x \\ y \end{bmatrix} \tag{10}$$

Here $\psi_{old}^{\mathscr{F}}\left(\vec{r}\right)$ is the wavefield in the Fourier-plane before the correction. The result is then propagated to the detector plane. In the detector plane the amplitude of the generated image is replaced

with the amplitude of the measured image. The modified image is then back-propagated to the lens where the inverse transfer function is applied.

$$\psi^{\mathscr{F}}_{corrected}(\vec{r}) = (1 - |T(\vec{r})|) \cdot \psi^{\mathscr{F}}_{old}(\vec{r}) + T^{*}(\vec{r}) \cdot \psi_{back}(\vec{r}) \tag{11}$$

* denotes the complex conjugate. Note that $|T| = 1$ for a perfect lens which is perfectly transparent and $|T| = 0$ outside the aperture. Finally the now corrected portion of the Fourier-plane is stitched into the original Fourier-plane from the guess:

$$\psi^{\mathscr{F}}_{new}(\vec{r}) = (1 - \alpha) \cdot \psi^{\mathscr{F}}_{old}(\vec{r}) + \alpha \cdot \psi^{\mathscr{F}}_{corrected}(\vec{r}) \tag{12}$$

The factor α is a noise factor that determines how much the wavefield should be changed and thus prevents noise in the measured image from dominating the new solution. $\alpha =]0, 1]$. $\alpha = 1$ would correspond to a image with no noise; a smaller alpha represents a image with more noise.
The process is then repeated for all measured images. Examples of how the lens positions cover the Fourier-plane can be seen in figure 4 and figure 5. The images must overlap in the Fourier-plane otherwise the reconstruction can't align the phase of individual images to a solution which is consistent with all measured images.
This process can then be repeated for any number of iterations and each time the error in the solution will be reduced. After doing one or several iterations the Fourier-plane can be back-propagated to the object-plane to show the reconstructed object. How correct the initial guess is affects the number of iterations needed to reach a solution with small error.

3.3 Updating the Transfer Function

Since the transfer function initially imitates a perfect lens with aperture then it won't match a real lens. It is possible to update the transfer function when applying a correction to Fourier-plane. [11] This will improve the reconstruction when the initial transfer function isn't correct.

$$T_{new}(\vec{r}) = T_{old}(\vec{r}) + \beta \cdot \frac{\psi^{*}_{\mathscr{F}}(\vec{r})}{max|\psi_{\mathscr{F}}(\vec{r})^{2}|} \cdot (\psi_{back}(\vec{r}) - \psi_{out}(\vec{r})) \tag{13}$$

The factor β is a noise factor, like α, that determines how much the transfer function should be changed.

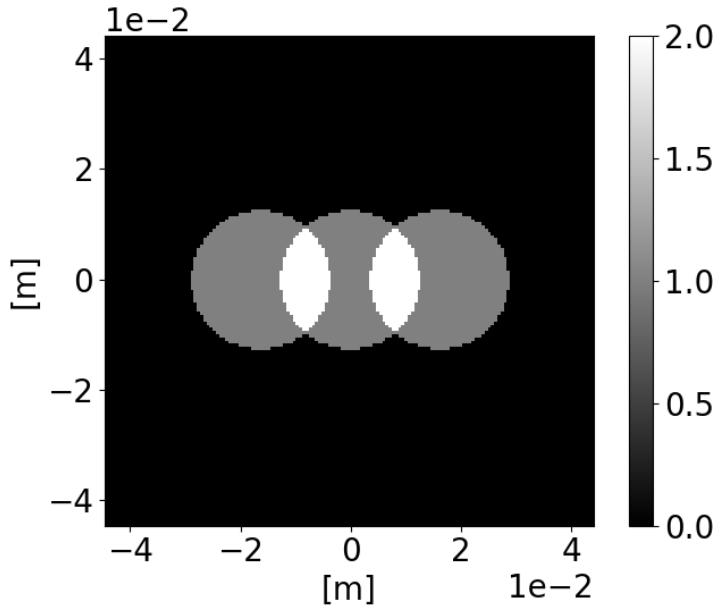

Figure 4: Coverage of the Fourier-plane using 3 images

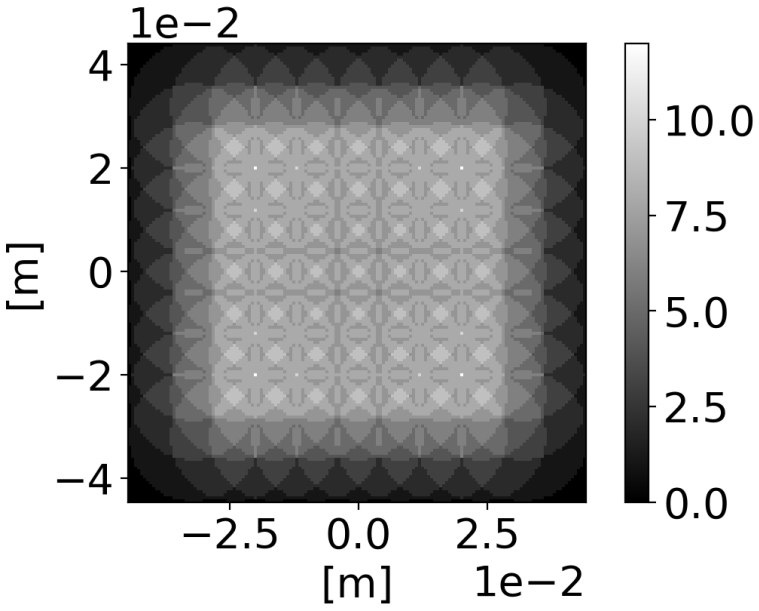

Figure 5: Coverage of the Fourier-plane using 81 images

Fourier Ptychography is here shown to reconstruct the transmission and phase using images simulated from a phantom. The parameters of the simulated experiment (except for the phantom and lens function) were set to match a real Fourier Ptychographic Microscopy setup. The phantom can be seen in figure 6. 81 images were forward simulated in the configuration shown in figure 5, some of the simulated images can be seen in figure 7. The reconstructed object after 1 and 10 iterations can be seen in figure 8. The phantom purposely has more pixels than what is possible for the reconstruction, this is to make sure that the reconstruction is limited by the quality of the method and simulated wavefield and not limited by the phantom.

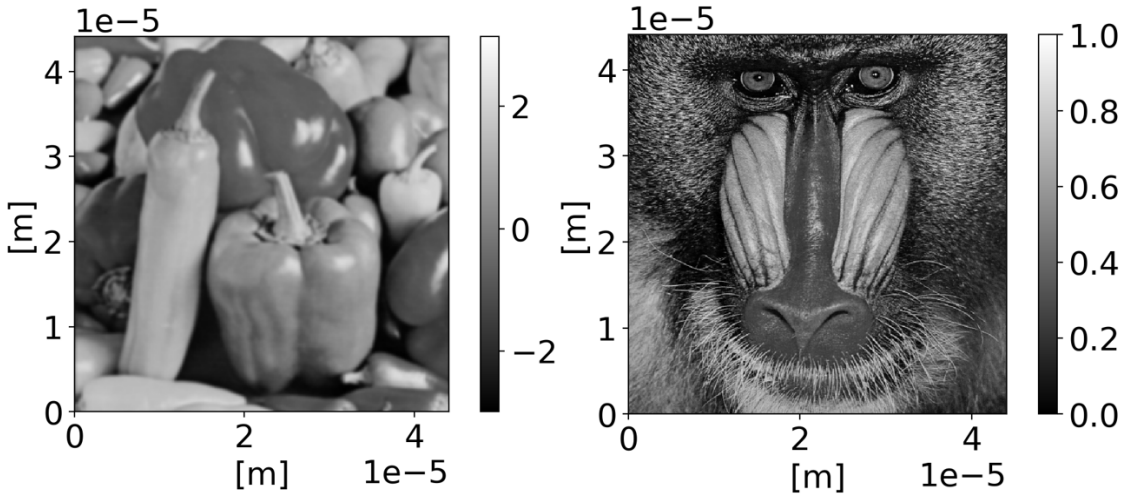

Figure 6: Phantom object. Left: Phase. Right: Intensity (512x512 pixels)

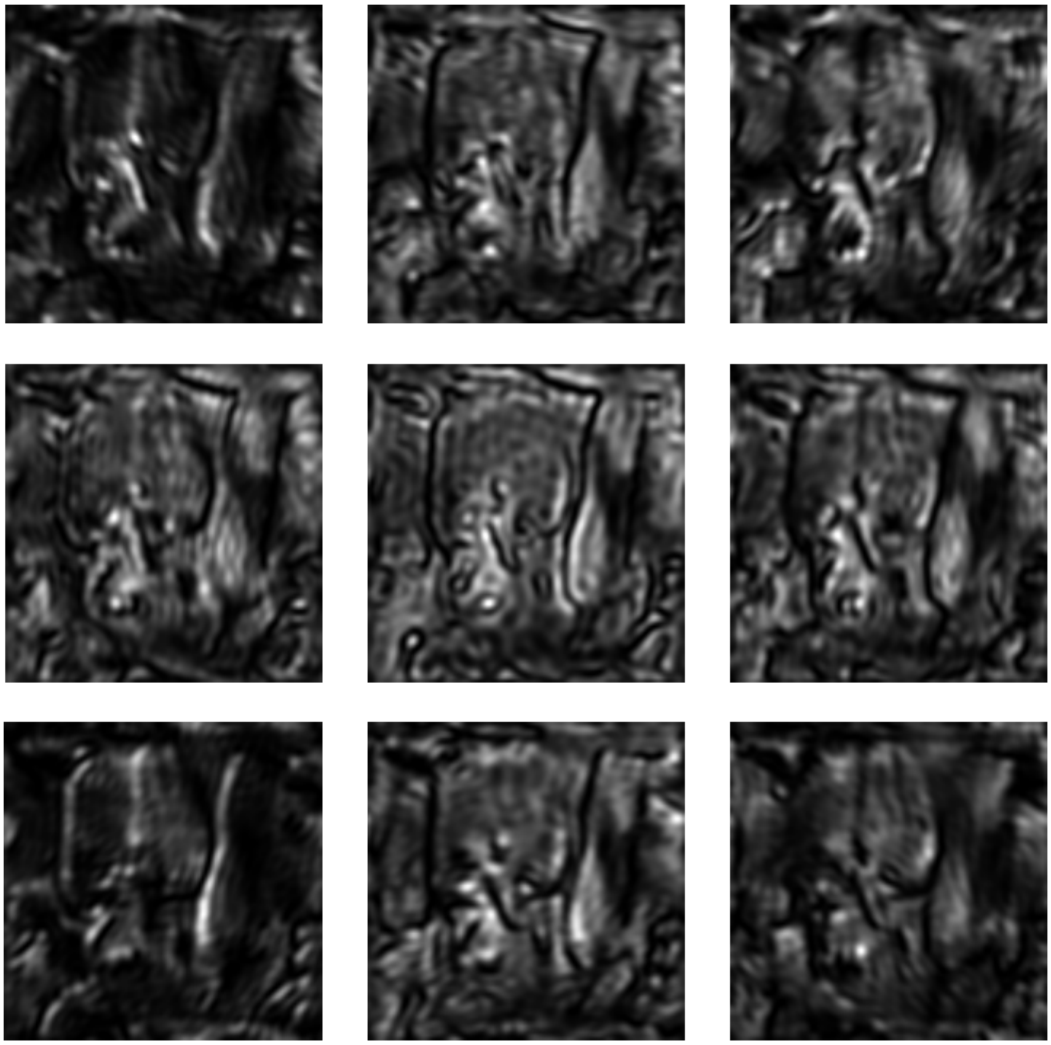

Figure 7: Small sample of the simulated images

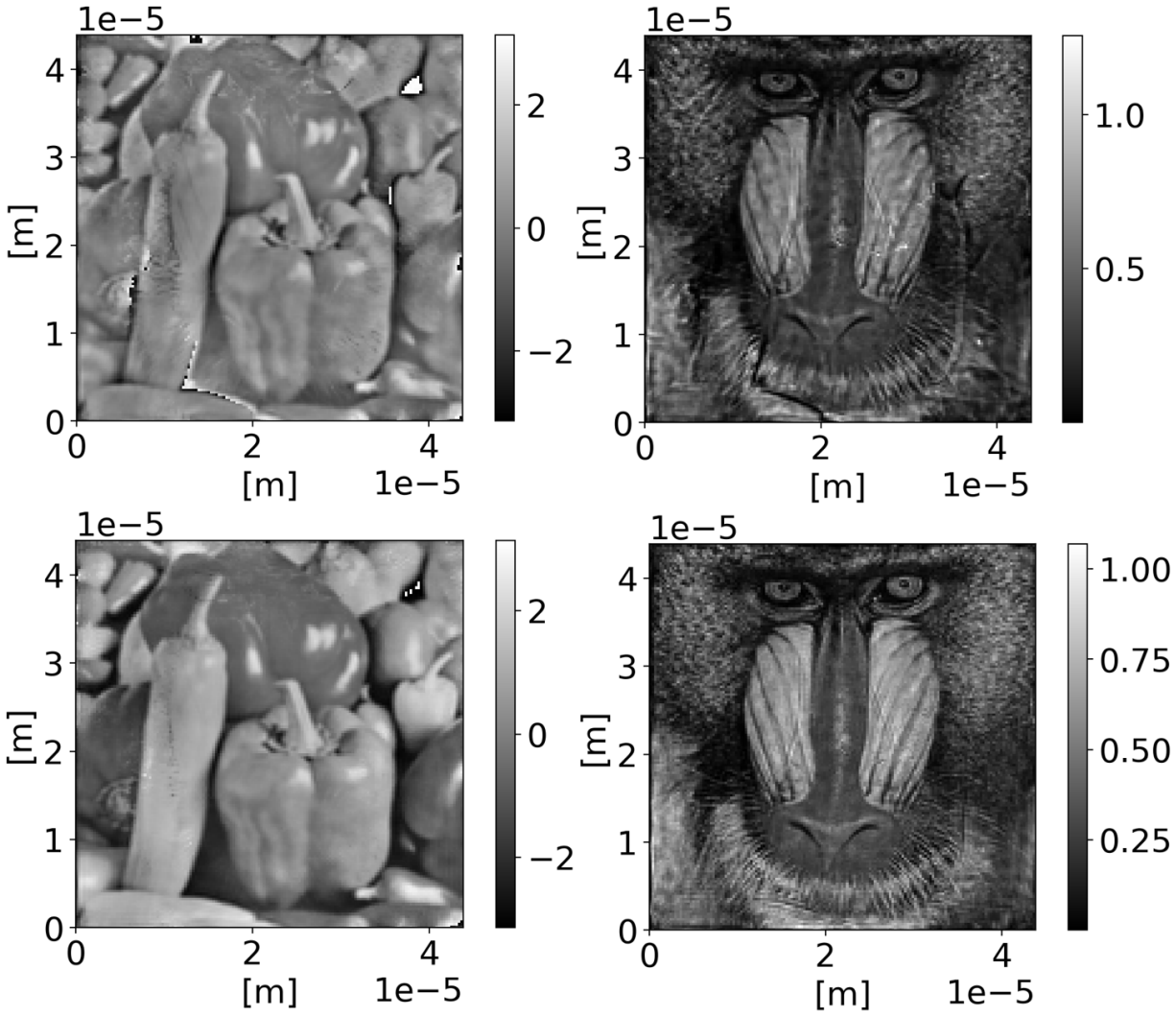

Figure 8: Reconstructed object. Top: After 1 iteration, Bottom: After 10 iterations (128x128 pixels)

3.4 Differential Phase Contrast

The sample phase can be reconstructed deterministically with a resolving power up to 2 times the NA of the lens. This is done by assuming that the transfer function is known and that the phase contribution can be isolated by using the weak object approximation:

$$\psi(\vec{r}) \approx 1 - \mu(\vec{r}) + i\phi(\vec{r}) \tag{14}$$

This leads to the following equation for the Fourier transform of the measured intensity [15]

$$\mathscr{F}(I(\vec{r})) = B\delta\left(\vec{r'}\right) + H_{abs}\left(\vec{r'}\right) \cdot \mathscr{F}(\mu(\vec{r})) + H_{ph}\left(\vec{r'}\right) \cdot \mathscr{F}(\phi(\vec{r})) \tag{15}$$

With two weak object transfer functions that apply for any pupil function (P) when the weak object approximation holds:

$$H_{abs}\left(\vec{r'}\right) = -P^*(\vec{s})\left(P(\vec{s}+\vec{r'}) + P(\vec{s}-\vec{r'})\right) \tag{16}$$

$$H_{ph}\left(\vec{r'}\right) = iP^*(\vec{s})\left(P(\vec{s}+\vec{r'}) - P(\vec{s}-\vec{r'})\right) \tag{17}$$

In this case the source is assumed to be a point source, this is not necessary but makes the transfer functions simpler by eliminating the source function. s is the lens position or the lens position that corresponds to the used illumination angle. The limitation of 2 NA originates from the limitations on s as set by the pupil function. Setting s outside the aperture results in the complex conjugated pupil function, $P^*(\vec{s})$, being zero and thus the transfer functions become zero and the intensity no longer depends on the sample.

The sample phase is calculated as an inverse problem where the difference between measurement and model is minimized. The measurement used here is the Differential Phase Contrast (DPC) image. This image is defined as the difference divided by the average intensity of any two measurements which are symmetric in lens translation: [15,20]

$$I_{DPC}(\vec{r}) = 2\frac{I_0(\vec{r}) - I_1(\vec{r})}{I_0(\vec{r}) + I_1(\vec{r})} \tag{18}$$

The model is that the Fourier transform of the DPC image depends linearly on the sample phase:

$$\mathscr{F}(I_{DPC}(\vec{r})) = H\left(\vec{r'}\right) \cdot \mathscr{F}(\phi(\vec{r})) \tag{19}$$

Where in the first derivative approximation the model function is assumed to be linear along the lens translation direction in the Fourier-plane. This means that Fourier components are multiplied

with a value representing their projection along this direction:

$$H\left(\vec{r'}\right) \approx i\vec{r'} \cdot (\vec{s_0} - \vec{s_1}) \tag{20}$$

The solution is the phase, $\phi(\vec{r})$, that minimizes the difference to all measured DPC images:[15]

$$min \sum_j \left| \mathscr{F}\left(I_{DPC,j}(\vec{r})\right) - H_j\left(\vec{r'}\right) \cdot \mathscr{F}\left(\phi(\vec{r})\right) \right|^2 + \alpha \left| \mathscr{F}\left(\phi(\vec{r})\right) \right|^2 \tag{21}$$

α is a noise factor that prioritizes solutions with smaller magnitude in the Fourier-plane. This equation can then be solved for the phase using Tikhonov regularization.
Compared to Fourier Ptychography this is much simpler to calculate as it doesn't require an iterative process and it doesn't require a starting guess. The disadvantages are that it is limited to 2 NA and it is impossible to correct the pupil function by updating the transfer function.

3.5 Fourier Ring Correlation

The problem of how to determine the level of detail arises when an image has been generated either trough direct measurement or indirect reconstruction. This is especially relevant when developing techniques with resolution beyond the resolving power of the lens since there is no obvious way to confirm whether the image is correct. The question is whether details beyond the resolving power of the lens are actually from the sample or whether they are artifacts of the method. Simulation has the unique advantage that the perfect result is known but a measure is still needed to determine how well a reconstruction fits with the initial phantom. For real samples a higher resolution technique can be used as basis for comparison. Fourier Ring Correlation is here used to quantitatively compare resolution of reconstructions from different methods and different measuring schemes.

$$FRC(q) = \frac{\sum_{\vec{q}} \mathscr{F}(I_0)\mathscr{F}(I_1)}{\sqrt{\sum_{\vec{q}} |\mathscr{F}(I_0)|^2} \sqrt{\sum_{\vec{q}} |\mathscr{F}(I_1)|^2}}, |\vec{q}| \in q \tag{22}$$

The Fourier Ring Correlation is a function of the size of the ring q. It is essentially calculating the correlation of band-passed images in Fourier space, which can then be shown as a function of spatial frequency. Note that I doesn't need to be intensity, it can be any image.
The resolution is here defined as the first time the Fourier Ring Correlation passes below $\frac{1}{7}$.[12] As can be seen in figure 11 this very closely responds to the width of one deviation of a Gaussian kernel.

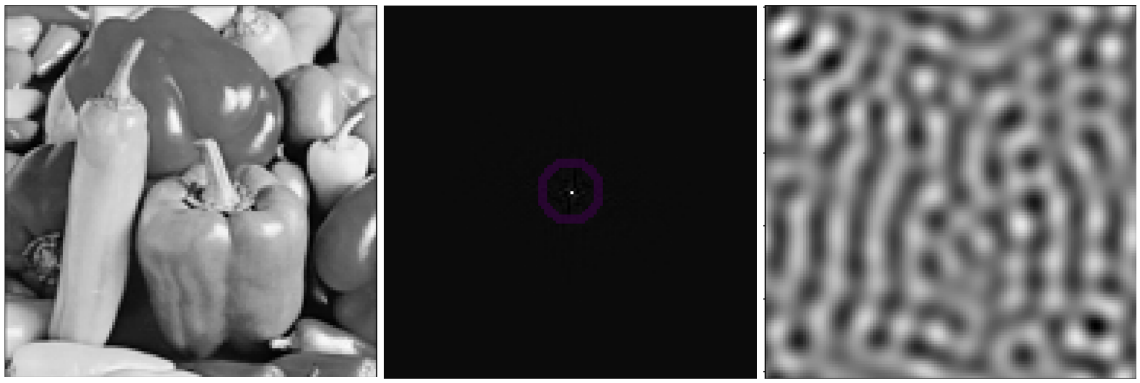

Figure 9: Left: original image, center: Fourier space overlaid with a Fourier-band, right: real-space representation of the Fourier band.

Figure 10: Left: original image, Right: image blurred by a Gaussian kernel with a radius of 2 pixels

The advantage of comparing the Fourier space of the images is that it doesn't require any previous knowledge about the sample structure.[12] One thing to note is that the Fourier Ring Correlation is independent of noise which doesn't obscure detail, this means noise at a smaller scale than the visible features won't change the quantitative measure of resolution.

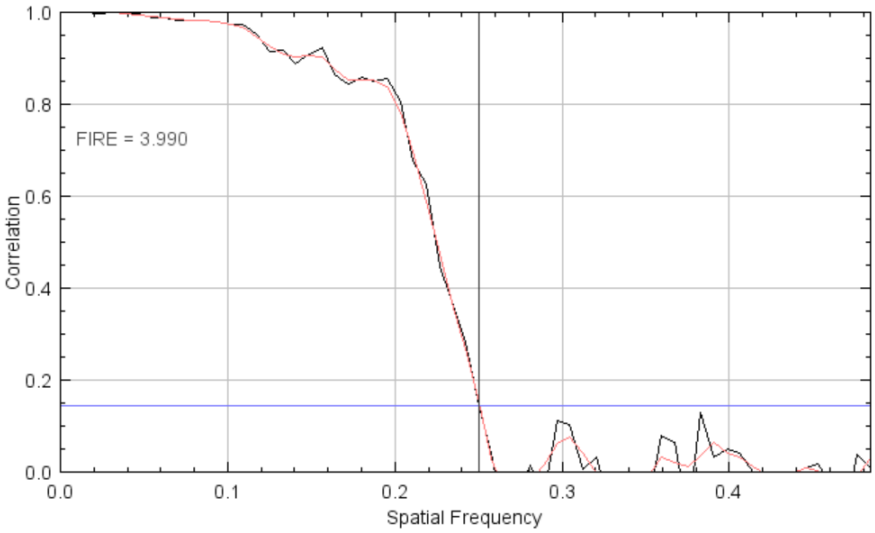

Figure 11: The Fourier Ring Correlation of the images in figure 10, The FIRE number given is the largest distance in pixels for which the correlation drops below $\frac{1}{7}$.

4 Aim & Hypothesis

The aim is to develop deterministic Fourier Ptychography as a method for high resolution reconstruction of phase contrast images. The method should provide a high resolution result comparable to Fourier Ptychography but without the long computation time that characterizes ptychography. This thesis proposes to use tilt aberration to achieve this. As shown at end of the appendix, successful use of the tilt aberration method allows reconstruction of the differential phase at arbitrary illumination angles or lens translation.[a] This is essential for the method proposed here. The new reconstruction of images at arbitrary NA suggests that it might somehow be possible to use stitching from Fourier Ptychography to combine more images to restore a high-resolution image of sample phase and transmittance. The method is promising in that it is applicable to both the visible light regime and X-rays. In the visible light regime it could serve as a easy way to increase resolving power without sacrificing FOV similar to Fourier Ptychography.

The project is split into smaller steps; first the use of tilt aberration must be generalized to combine several images with arbitrary lens position. Second, the differential phase must be integrated to

[a] lens translation will from this point onward refer to both the use of illumination angles and lens translation for the tilt aberration method. Figure 3, figure 4 and figure 5 shows the intuition behind this choice

phase. Third, the resolution must be increased beyond the resolution of individual images. While the project is approached in this order to make use of the results of ptychography it could be of interest to investigate whether the phase or differential phase in the sample plane could be extracted without integration as is done in Differential Phase Contrast.

5 Deterministic Differential Phase

5.1 Non-Collinear Lens Translation

Adding more images collinear with the previous can be done by expanding the finite difference used in the appendix. But this group of images contain no information in the direction perpendicular to their relative translation. The case of interest is where at least one is non-collinear with the rest. The most practical solution to this is to expand the use of the tilt aberration method to an arbitrary number of images at arbitrary lens translation. Rather than using finite difference the differential phase can be determined as an inverse problem of linear equations for intensity at different lens positions. This is done by writing the logarithm to intensity as a model of differential phase; rewriting equation 199:

$$\frac{\partial \log\left(I\left(\vec{r}\right)\right)}{\partial \tau} = -4\pi\gamma\nabla_{\perp}\phi\left(\vec{r}\right) \tag{23}$$

$$\updownarrow$$

$$\log\left(I\left(\vec{r}\right)\right) = -4\pi\gamma\int \nabla_{\perp}\phi\left(\vec{r}\right)d\tau \tag{24}$$

Assuming the differential phase at the detector doesn't change as a function of tilt:

$$\frac{\partial}{\partial \tau}\nabla_{\perp}\phi\left(\vec{r}\right) = 0 \tag{25}$$

This corresponds to the requirement that the sample projection on the detector must remain stationary and the sample cannot change between measurements at different tilt. Note that the intensity and phase will change as function of tilt but the differential phase cannot. Using this assumption the differential phase isn't a funciton of tilt and thus eq. 24 becomes:

$$\log\left(I\left(\vec{r}\right)\right) = -4\pi\gamma\tau\nabla_{\perp}\phi\left(\vec{r}\right) + C\left(\vec{r}\right) \tag{26}$$

Taking n measurements of intensity at arbitrary lens translation results in n linear equations. This is written in vector notation where the content of each vector is made explicit to show how each

measured intensity arises from a lens translation and the differential phase which is independent of translation:

$$\begin{pmatrix} \log(I_1(\vec{r})) \\ \log(I_2(\vec{r})) \\ \vdots \\ \log(I_n(\vec{r})) \end{pmatrix} = -4\pi\gamma \begin{pmatrix} \tau_{1x} & \tau_{1y} \\ \tau_{2x} & \tau_{2y} \\ \vdots & \vdots \\ \tau_{nx} & \tau_{ny} \end{pmatrix} \begin{pmatrix} \frac{\partial\phi(\vec{r})}{\partial x} \\ \frac{\partial\phi(\vec{r})}{\partial y} \end{pmatrix} + C(\vec{r}) \tag{27}$$

The goal of the inverse problem is now to determine the differential phase which results in the best match to the measured intensities. To this end the tikhonov regularization is used since it determines the least squares solution to an inverse problem and allows for noise reduction by prioritizing a result with smaller magnitude.

Using Tikonov reg. the detected intensities, $\vec{d}$, are given as a linear function of the model parameters, $\vec{m}$:

$$\vec{d}(\vec{r}) = A\vec{m}(\vec{r}) \tag{28}$$

The optimal model parameters for a given model and measurements are:

$$\vec{m}(\vec{r}) = (A^T A - \varepsilon^2 I)^{-1} A^T \vec{d}(\vec{r}) \tag{29}$$

I is the identity matrix.

To validate the method under controlled conditions an imaging setup is simulated with propagation based on equation 5 and it is assumed that the Fresnel number is much less than 1. This imaging setup is used for all simulations in this project to make sure that results are comparable. The Fourier ptychographic method of tilting the incident light is chosen as the focus since it serves as the easier way to get access to experimental data. The simulated setup contains a $640nm$ coherent source and a lens with an aperture radius of $3.145mm$. The distance from sample to lens is $10mm$ while the distance from lens to detector is $100mm$. The focal length of the lens is $9.0909mm$, using equation 8 it can be seen that the sample is in focus. The NA of the lens is 0.3 which by eq. 2 leads to a smallest resolvable detail of $1.07\mu m$. The simulated phantom is shown in figure 6. The wavefield from the phantom is propagated through the imaging system from 25 different source angles corresponding to 25 bright-field measurements and then again at 25 angles corresponding to a mix of bright-field and dark-field. The resulting 2 sets of 25 images are reconstructed separately; both the differential phase and the constant C from equation 27 is reconstructed. The reconstruction for each pixel is shown in figure 12 for the bright-field images and in figure 13 for the set containing

both bright-field and dark-field. A dark-field image is defined as an image where no background intensity is measured as only scattering from the sample is detected. The images are dark-field in this setup when the illumination angle is so large that the direct beam no longer reaches the detector.

For the set containing only bright-field images the resolution of the reconstructed phase from Fourier Ring Correlation is $16.5\mu m$ while the phase from the mixed set has a resolution of $16.8\mu m$. The loss of resolution is minor since the noise induced in the mixed field case is at a smaller scale than the smallest resolved feature.

It is possible to show the result of Tikhonov regularization in a single pixel as a fit to the measured intensity. Doing this with the mixed dataset, Figure 14, shows that the tilt aberration method doesn't accurately describe the intensities from simulation when combining bright-field and dark-field.

Equation 27 leads to a result similar to the first derivative approximation of Differential Phase Contrast. The method is very noise sensitive since a relatively small change in intensity at large lens translation will cause a large change in the differential phase. It should also be noted that using a dataset which doesn't have an average lens position of 0 will bias the result, see figure 15. The result should depend on measurement but not be biased by the location of the measurement. This means the method will not work for stitching since it must work for a group of measurements at any lens position.

These problems arise from the use of a shift-invariant system when describing aberration space as used for determining phase from tilt aberration. In the definition of aberration space it is explicitly assumed that:[21]

$$C_{mn}^{(I)} \geq 0 \text{ for all m and n} \tag{30}$$

$$C_{mn}^{(I)} = 0 \text{ if m and/or n is odd} \tag{31}$$

Both these assumptions contradict equation 185 used during definition of tilt aberration. Tilt aberration requires that the system isn't shift-invariant as translating the input wavefield should lead to dark-field images and not a translated image of the sample. The algebraic reason is that γ becomes zero when the lens is infinite corresponding to a shift-invariant system. That γ becomes zero is shown in the following section and a solution is presented.

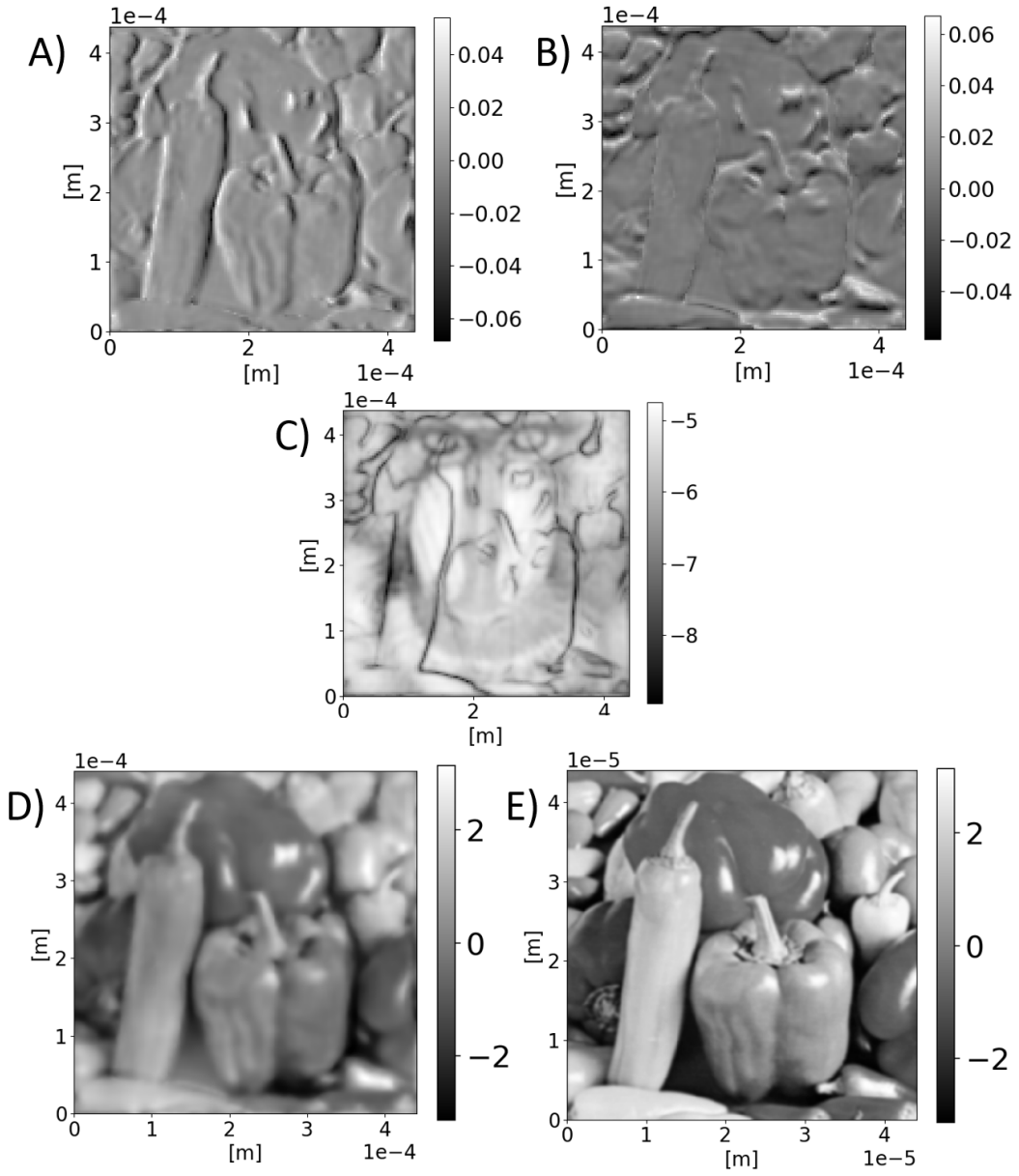

Figure 12: Reconstruction from 25 images taken in bright-field. A: reconstructed phase differential along x. B: reconstructed phase differential along y. C: the reconstructed constant C. D: integration of phase differentials. E: original phase

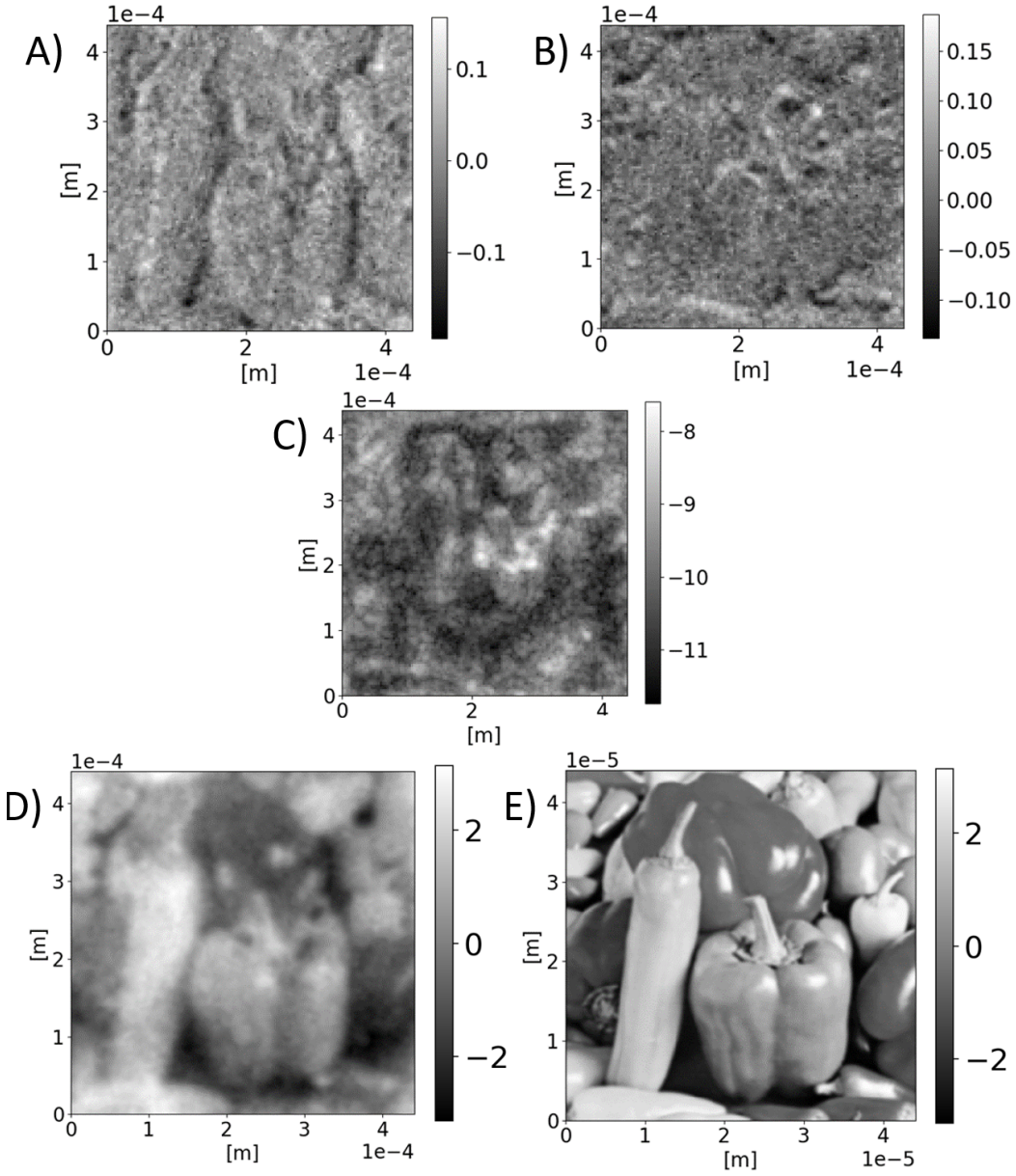

Figure 13: Reconstruction from 25 images taken in a mix of bright-field and dark-field. A: reconstructed phase differential along x. B: reconstructed phase differential along y. C: the reconstructed constant C. D: integration of phase differentials. E: original phase

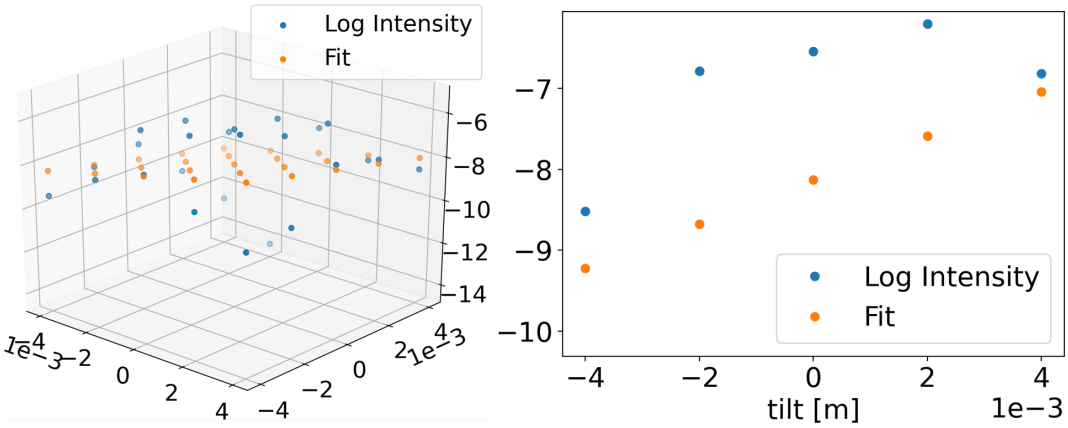

Figure 14: The least squares solution to equation 27 found by Tikhonov regularization. $\frac{\partial\phi(\vec{r})}{\partial x}$ and $\frac{\partial\phi(\vec{r})}{\partial y}$ determine the slope of the fit in the x and y-direction respectively. The tilt aberration theory used for equation 27 predicts the logarithm of the intensity to be linear in lens translation. Left: fit shown as a function of tilt in both x and y. Every pixel of the reconstruction has a fit like this as a function of 2 variables, but it is hard to see if the fit is good. Right: fit shown along one dimension by only showing measurements where the tilt along the other dimension is 0. It can be seen that the logarithm of the intensity is not linear in tilt. The first derivative approximation of Differential Phase Contrast works as it can be approximated as linear close to 0 tilt.

5.2 Gaussian Aperture

Explicitly calculating the effects of the imaging system and including an aperture with a Gaussian transmission function makes it possible to determine an approximation for γ. For this reason a Gaussian apodizer is used, it is essentially a filter with a Gaussian transmission function centered in the middle of the filter. The lens is still finite but the approximation of infinite Gaussian transmission for a Gaussian apodizer and finite lens is much better than the approximation of an infinite lens for a finite lens. The wavefield in the detector plane can be written as the result of several actions applied sequentially to the initial wavefield. First the wavefield is propagated to the lens plane by the Fresnel-Kirchoff integral, equation 143. Then the Gaussian function $A\left(r_1, s\right)$, at lens position s, is applied to the wavefield. Finally the wavefield is propagated to the detector plane, again by the Fresnel-Kirchoff integral. For the sake of simplicity the derivation is shown with

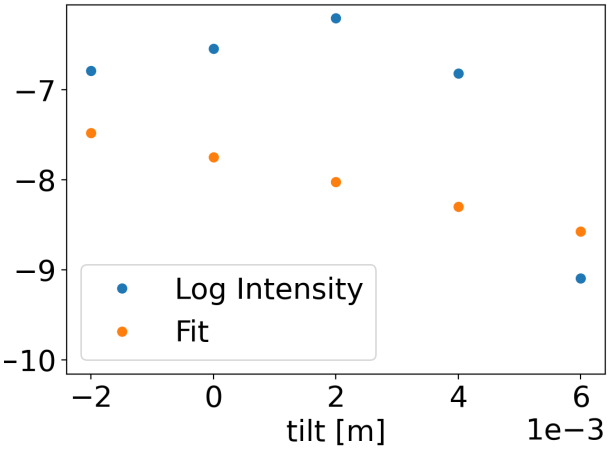

Figure 15: Fit of the same pixel as figure 14 but now the slope is different as there are more measurements in the positive direction than in the negative direction.

only one transverse dimension.

$$\psi_2 = Q_2\left(r_2, s\right)\mathscr{F}^{-1}\left(A\left(r_1, s\right)Q_1\left(r_1\right)\mathscr{F}\left(\psi_0\left(r_0\right)Q_0\left(r_0\right)\right)\right) \tag{32}$$

$$A\left(r_1, s\right) = \exp\left(-\frac{\left(r_1 - s\right)^2}{2\sigma^2}\right) \tag{33}$$

Where Q_0, Q_1 and Q_2 are the quadratic phase factors from the Fresnel-Kirchoff integral. Q_2 also includes the effect of the lens:

$$Q_2\left(r_2, s\right) = \exp\left(i\frac{k}{2z_2}\left(r_2^2 - s^2\left(\frac{z_2}{z_1} + 1\right)\right)\right) \tag{34}$$

Differentiating with respect to lens position and expanding using the product rule:

$$\begin{aligned}\frac{\partial\psi_2}{\partial s} = \frac{\partial Q_2\left(r_2, s\right)}{\partial s}\mathscr{F}^{-1}\left(A\left(r_1, s\right)Q_1\left(r_1\right)\mathscr{F}\left(\psi_0\left(r_0\right)Q_0\left(r_0\right)\right)\right)\cdot \\ Q_2\left(r_2, s\right)\frac{\partial}{\partial s}\mathscr{F}^{-1}\left(A\left(r_1, s\right)Q_1\left(r_1\right)\mathscr{F}\left(\psi_0\left(r_0\right)Q_0\left(r_0\right)\right)\right)\end{aligned} \tag{35}$$

Differentiating Q_2:

$$\frac{\partial Q_2\left(r_2, s\right)}{\partial s} = -i\frac{ks}{z_2}\left(\frac{z_2}{z_1} + 1\right)Q_2\left(r_2, s\right) \tag{36}$$

Thus:

$$\frac{\partial Q_2\left(r_2, s\right)}{\partial s}\mathscr{F}^{-1}\left(A\left(r_1, s\right)Q_1\left(r_1\right)\mathscr{F}\left(\psi_0\left(r_0\right)Q_0\left(r_0\right)\right)\right) = -i\frac{ks}{z_2}\left(\frac{z_2}{z_1} + 1\right)\psi_2 \tag{37}$$

$A(r_1, s)$ is the only term in the inverse Fourier transform that depends on the lens position. The differentiation with respect to lens position can be moved inside the Fourier transform since it applies to a different variable:

$$\frac{\partial}{\partial s}\mathscr{F}^{-1}\left(A(r_1,s)\,Q_1(r_1)\,\mathscr{F}\left(\psi_0(r_0)\,Q_0(r_0)\right)\right) = \mathscr{F}^{-1}\left(\frac{\partial A(r_1,s)}{\partial s}Q_1(r_1)\,\mathscr{F}\left(\psi_0(r_0)\,Q_0(r_0)\right)\right) \tag{38}$$

$$\frac{\partial A(r_1,s)}{\partial s} = \frac{\partial}{\partial s}\exp\left(-\frac{(r_1-s)^2}{2\sigma^2}\right) \tag{39}$$

Expanding the quadratic term and separating into different exponentials:

$$\frac{\partial A(r_1,s)}{\partial s} = \frac{\partial}{\partial s}\left(\exp\left(-\frac{r_1^2}{2\sigma^2}\right)\exp\left(-\frac{s^2}{2\sigma^2}\right)\exp\left(\frac{r_1 s}{\sigma^2}\right)\right) \tag{40}$$

$$\updownarrow$$

$$\frac{\partial A(r_1,s)}{\partial s} = \exp\left(-\frac{r_1^2}{2\sigma^2}\right)\left(-\frac{s}{\sigma^2}\exp\left(-\frac{s^2}{2\sigma^2}\right)\exp\left(\frac{r_1 s}{\sigma^2}\right) + \frac{r_1}{\sigma^2}\exp\left(-\frac{s^2}{2\sigma^2}\right)\exp\left(\frac{r_1 s}{\sigma^2}\right)\right) \tag{41}$$

$$\updownarrow$$

$$\frac{\partial A(r_1,s)}{\partial s} = A(r_1,s)\left(\frac{r_1}{\sigma^2} - \frac{s}{\sigma^2}\right) \tag{42}$$

Thus:

$$\begin{aligned} &Q_2(r_2,s)\,\frac{\partial}{\partial s}\mathscr{F}^{-1}\left(A(r_1,s)\,Q_1(r_1)\,\mathscr{F}\left(\psi_0(r_0)\,Q_0(r_0)\right)\right) = \\ &-\frac{s}{\sigma^2}\psi_2 + \frac{Q_2}{\sigma^2}\mathscr{F}^{-1}\left(r_1 A(r_1,s)\,Q_1(r_1)\,\mathscr{F}\left(\psi_0(r_0)\,Q_0(r_0)\right)\right) \end{aligned} \tag{43}$$

Substituting eq. 37 and 43 into eq. 35:

$$\frac{\partial \psi_2}{\partial s} = -i\frac{ks}{z_2}\left(\frac{z_2}{z_1}+1\right)\psi_2 - \frac{s}{\sigma^2}\psi_2 + \frac{Q_2}{\sigma^2}\mathscr{F}^{-1}\left(r_1 A(r_1,s)\,Q_1(r_1)\,\mathscr{F}\left(\psi_0(r_0)\,Q_0(r_0)\right)\right) \tag{44}$$

Want to find a function $f(r_2)$ for which:

$$\frac{\partial f(r_2)}{\partial r_2} = \mathscr{F}^{-1}\left(r_1 A(r_1,s)\,Q_1(r_1)\,\mathscr{F}\left(\psi_0(r_0)\,Q_0(r_0)\right)\right) \tag{45}$$

This is useful since the angular frequency of r_2 can be directly related to r_1 in the Fraunhofer regime and the Fourier derivative theorem can be used to eliminate the outer Fourier transform:

$$\mathscr{F}\left(\frac{\partial f(r_2)}{\partial r_2}\right) = i\omega\mathscr{F}\left(f(r_2)\right) \tag{46}$$

$$\updownarrow$$

$$\frac{\partial f(r_2)}{\partial x} = \mathscr{F}^{-1}\left(i\omega \mathscr{F}\left(f(r_2)\right)\right) \tag{47}$$

Inserting $\frac{\partial f(r_2)}{\partial r_2}$:

$$\mathscr{F}^{-1}\left(r_1 A\left(r_1, s\right) Q_1\left(r_1\right) \mathscr{F}\left(\psi_0\left(r_0\right) Q_0\left(r_0\right)\right)\right) = \mathscr{F}^{-1}\left(i\omega \mathscr{F}\left(f(r_2)\right)\right) \tag{48}$$

$$\updownarrow$$

$$r_1 A\left(r_1, s\right) Q_1\left(r_1\right) \mathscr{F}\left(\psi_0\left(r_0\right) Q_0\left(r_0\right)\right) = i\omega \mathscr{F}\left(f(r_2)\right) \tag{49}$$

$$\updownarrow$$

$$\mathscr{F}^{-1}\left(\frac{r_1}{i\omega} A\left(r_1, s\right) Q_1\left(r_1\right) \mathscr{F}\left(\psi_0\left(r_0\right) Q_0\left(r_0\right)\right)\right) = f(r_2) \tag{50}$$

In the Fraunhofer regime the angular frequency of r_2 is:

$$\omega = \frac{r_1 k}{z_2} \tag{51}$$

Substituting into eq. 50:

$$f(r_2) = \frac{z_2}{ik} \mathscr{F}^{-1}\left(A\left(r_1, s\right) Q_1\left(r_1\right) \mathscr{F}\left(\psi_0\left(r_0\right) Q_0\left(r_0\right)\right)\right) \tag{52}$$

$$\updownarrow$$

$$f(r_2) = \frac{z_2}{ik} \frac{\psi_2}{Q_2} \tag{53}$$

Differentiating with respect to r_2:

$$\frac{\partial f(r_2)}{\partial r_2} = \frac{z_2}{ik} \frac{\partial}{\partial r_2} \frac{\psi_2}{Q_2} \tag{54}$$

Inserting from eq. 45:

$$\mathscr{F}^{-1}\left(r_1 A\left(r_1, s\right) Q_1\left(r_1\right) \mathscr{F}\left(\psi_0\left(r_0\right) Q_0\left(r_0\right)\right)\right) = -\frac{iz_2}{k} \frac{\partial}{\partial r_2} \frac{\psi_2}{Q_2} \tag{55}$$

Expanding using the product rule:

$$\mathscr{F}^{-1}\left(r_1 A\left(r_1, s\right) Q_1\left(r_1\right) \mathscr{F}\left(\psi_0\left(r_0\right) Q_0\left(r_0\right)\right)\right) = -\frac{iz_2}{k}\left(\frac{\partial \psi_2}{\partial r_2} \frac{1}{Q_2\left(r_2, s\right)} + \frac{\partial \left(Q_2\left(r_2, s\right)\right)^{-1}}{\partial r_2} \psi_2\right) \tag{56}$$

Differentiating the inverse of Q_2 from eq. 34:

$$\frac{\partial \left(Q_2\left(r_2, s\right)\right)^{-1}}{\partial r_2} = -i\frac{k r_2}{z_2} \frac{1}{Q_2\left(r_2, s\right)} \tag{57}$$

Substituting into eq. 56:

$$\mathscr{F}^{-1}\left(r_1 A\left(r_1, s\right) Q_1\left(r_1\right) \mathscr{F}\left(\psi_0\left(r_0\right) Q_0\left(r_0\right)\right)\right) = -\frac{i z_2}{k Q_2}\left(\frac{\partial \psi_2}{\partial r_2} - i\frac{k r_2}{z_2}\psi_2\right) \tag{58}$$

$$\updownarrow$$

$$\mathscr{F}^{-1}\left(r_1 A\left(r_1, s\right) Q_1\left(r_1\right) \mathscr{F}\left(\psi_0\left(r_0\right) Q_0\left(r_0\right)\right)\right) = -\frac{1}{Q_2}\left(\frac{i z_2}{k}\frac{\partial \psi_2}{\partial r_2} + r_2\psi_2\right) \tag{59}$$

Inserting in eq. 44:

$$\frac{\partial \psi_2}{\partial s} = -i\frac{ks}{z_2}\left(\frac{z_2}{z_1}+1\right)\psi_2 - \frac{s}{\sigma^2}\psi_2 - \frac{1}{\sigma^2}\left(\frac{i z_2}{k}\frac{\partial \psi_2}{\partial r_2} + r_2\psi_2\right) \tag{60}$$

The wavefunction is substituted for its exponential form and multiplied by its complex conjugate similar to what is done for eq. 192 in the appendix:

$$\psi_2 = \sqrt{I}\exp\left(i\phi\right) \tag{61}$$

$$\psi_2^* = \sqrt{I}\exp\left(-i\phi\right) \tag{62}$$

$$\sqrt{I}\frac{\partial\sqrt{I}}{\partial s} + iI\frac{\partial\phi}{\partial s} = -i\frac{ks}{z_2}\left(\frac{z_2}{z_1}+1\right)I - \frac{s}{\sigma^2}I - \frac{i z_2}{k\sigma^2}\left(\sqrt{I}\frac{\partial\sqrt{I}}{\partial r_2} + iI\frac{\partial\phi}{\partial r_2}\right) - \frac{r_2}{\sigma^2}I \tag{63}$$

$$\updownarrow$$

$$\sqrt{I}\frac{\partial\sqrt{I}}{\partial s} + iI\frac{\partial\phi}{\partial s} = -i\frac{ks}{z_2}\left(\frac{z_2}{z_1}+1\right)I - \frac{s}{\sigma^2}I - \frac{i z_2\sqrt{I}}{k\sigma^2}\frac{\partial\sqrt{I}}{\partial r_2} + \frac{I z_2}{k\sigma^2}\frac{\partial\phi}{\partial r_2} - \frac{r_2}{\sigma^2}I \tag{64}$$

Isolating the real parts since all variables are defined to be real:

$$\sqrt{I}\frac{\partial\sqrt{I}}{\partial s} = -\frac{s}{\sigma^2}I + \frac{I z_2}{k\sigma^2}\frac{\partial\phi}{\partial r_2} - \frac{r_2}{\sigma^2}I \tag{65}$$

Dividing by I by assuming $I > 0$:

$$\frac{1}{\sqrt{I}}\frac{\partial\sqrt{I}}{\partial s} = -\frac{s}{\sigma^2} + \frac{z_2}{k\sigma^2}\frac{\partial\phi}{\partial r_2} - \frac{r_2}{\sigma^2} \tag{66}$$

$$\updownarrow$$

$$\frac{1}{2}\frac{\partial\log I}{\partial s} = -\frac{s}{\sigma^2} + \frac{z_2}{k\sigma^2}\frac{\partial\phi}{\partial r_2} - \frac{r_2}{\sigma^2} \tag{67}$$

$$\updownarrow$$

$$\log I = \int ds \left(-\frac{2s}{\sigma^2} + \frac{2z_2}{k\sigma^2}\frac{\partial \phi}{\partial r_2} - \frac{2r_2}{\sigma^2} \right) \tag{68}$$

Using the assumption in eq. 25:

$$\log I = -\frac{s^2}{\sigma^2} + \frac{2z_2}{k\sigma^2}\frac{\partial \phi}{\partial r_2}s - \frac{2r_2}{\sigma^2}s + C \tag{69}$$

the lens position, s, becomes the tilt, τ, when using the notation from tilt aberration. It can be seen that the factor in front of $\frac{\partial \phi}{\partial r_2}\tau$ is now $\frac{2z_2}{k\sigma^2}$ instead of $-4\pi\gamma$ as in eq. 26. Letting the lens aperture become infinite without a gaussian apodizer must be identical to letting σ approach infinity with the gaussian apodizer. This shows that γ must go to zero as the lens aperture becomes infinite:

$$\lim_{\sigma\to\infty} -4\pi\gamma \propto \lim_{\sigma\to\infty} \frac{2z_2}{k\sigma^2} = 0 \tag{70}$$

Using eq. 69 the system of linear equations is:

$$\begin{pmatrix} \log(I_1) \\ \log(I_2) \\ \vdots \\ \log(I_n) \end{pmatrix} = -\begin{pmatrix} \tau_1^2 \\ \tau_2^2 \\ \vdots \\ \tau_n^2 \end{pmatrix} \sigma^{-2} + \frac{2}{\sigma^2} \begin{pmatrix} \tau_{1x} & \tau_{1y} \\ \tau_{2x} & \tau_{2y} \\ \vdots & \vdots \\ \tau_{nx} & \tau_{ny} \end{pmatrix} \cdot \left(\begin{pmatrix} \frac{\partial \phi}{\partial x} \\ \frac{\partial \phi}{\partial y} \end{pmatrix} \frac{z_2}{k} - \begin{pmatrix} r_{2x} \\ r_{2y} \end{pmatrix} \right) + C \tag{71}$$

The only unknown is the differential phase. Moving all known terms to the left hand side and absorbing them in a single vector:

$$\vec{d} = \frac{2z_2}{k\sigma^2} \begin{pmatrix} \tau_{1x} & \tau_{1y} \\ \tau_{2x} & \tau_{2y} \\ \vdots & \vdots \\ \tau_{nx} & \tau_{ny} \end{pmatrix} \cdot \begin{pmatrix} \frac{\partial \phi}{\partial x} \\ \frac{\partial \phi}{\partial y} \end{pmatrix} + C \tag{72}$$

The reconstruction is again done in two dimensions for each pixel. In figure 16 it can be seen that using the Gaussian apodizer with equation 69 produces a much better fit. It isn't supposed to be a perfect fit as different areas of the Fourier-plane should reveal new information about the sample.

5.3 Restoring Beam Angles

The differential phase should contain a contribution from the angled beam when using the Fourier ptychographic method of angling the incident beam, see figure 17. This isn't a problem in normal Fourier Ptychography as the angle contribution to the phase is retained from the propagation to

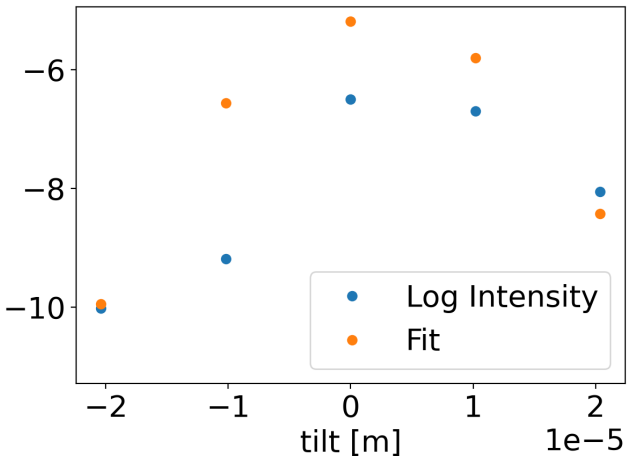

Figure 16: The least squares solution to equation 69 found by Tikhonov regularization. Fit of the same pixel as figure 14 and figure 15.

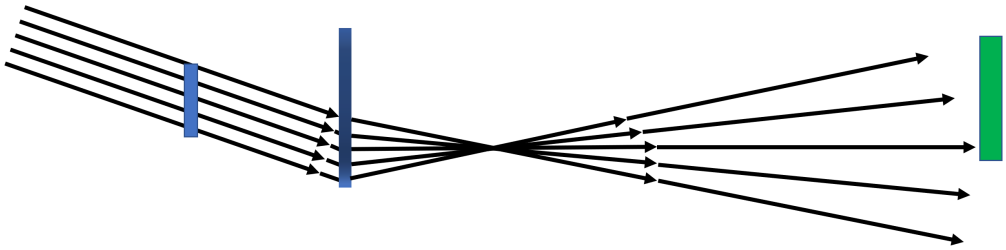

Figure 17: Sketch of the experimentally inherent phase differential across the detector that arises from an angled incident wave. The length of the arrows represent the wavelength and it doesn't change.

the detector plane. Only the amplitude of the wavefield is corrected in the detector plane. However, when using Deterministic Fourier Ptychography it isn't known if the differential phase contribution from the angle is correct. It is possible to re-add the contribution from the angled beam by assuming that the phase change incurred by the sample is independent of the beam angle. This assumption is already a premise of Fourier Ptychography in that the angled illumination is assumed to just cause a translation of the wavefield in the Fourier-plane. The assumption is that the differential phase can be split in two terms, one from the sample ($\nabla_\perp \phi_s$) and one from the angle ($\nabla_\perp \phi_\theta$):

$$\nabla_\perp \phi = \nabla_\perp \phi_s + \nabla_\perp \phi_\theta \tag{73}$$

The differential phase contribution from the angled beam is here determined by forward simulation without a sample since the experimental parameters are known exactly. The forward simulation uses the propagation derived in equation 5. The wavefield from the forward simulation is normalized so it doesn't affect intensity and then it is multiplied with the reconstructed wavefield to add the phase:

$$\psi = \psi_0 \cdot \frac{\psi_\theta}{|\psi_\theta|} \tag{74}$$

In figure 18 it can be seen what happens when back-propagation is done with or without adding a contribution from the angled beam. The contribution is currently added during reconstruction. However, completely ignoring the angle might lead to a useful result. Figure 19 shows the result of attempting to deterministically stitch wavefields without changing the angle. This leads to a result that resembles the sample but the artifacts have yet to successfully be removed. One reason might be that the reconstructions obtain an imperfect mean angle from measurements during reconstruction in the detector-plane.

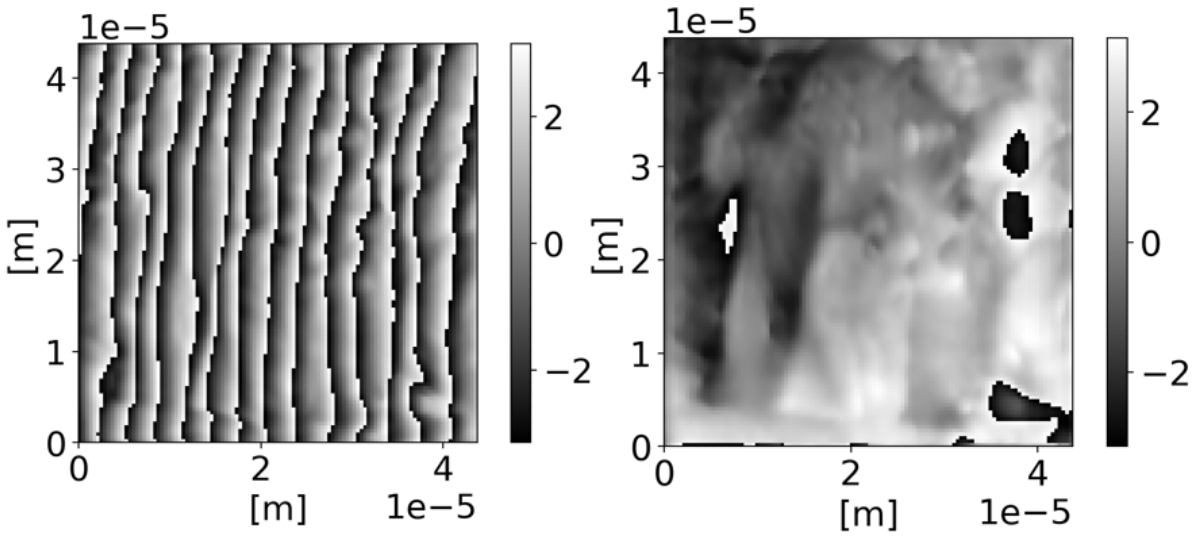

Figure 18: Left: back-propagating a wavefield to the sample-plane without adding phase contribution from the angled wavefield in the detector-plane. Right: back-propagating after adding phase as determined from forward simulation without a sample.

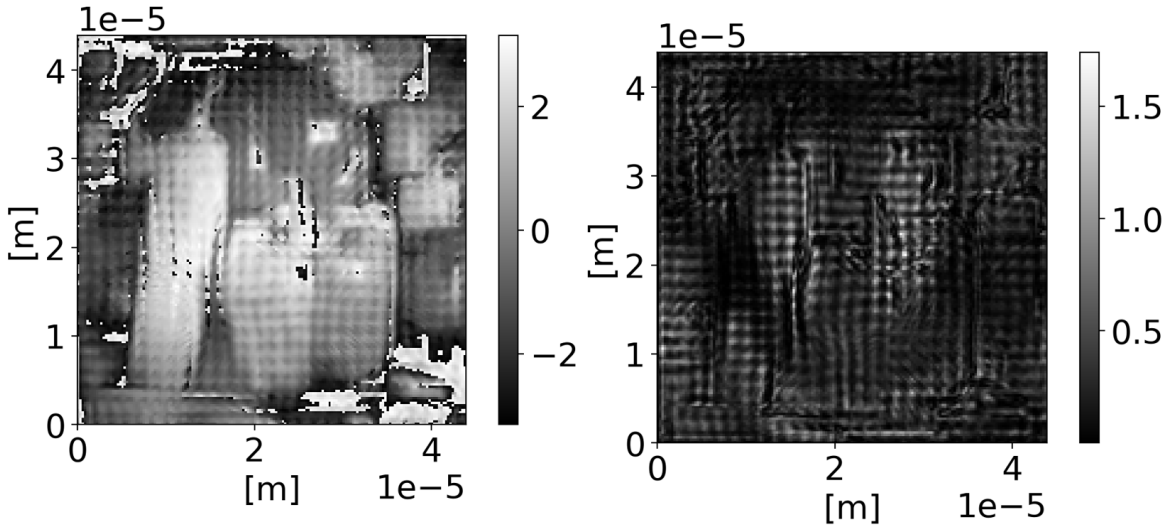

Figure 19: Stitching the Fourier-plane and back-propagating to the sample-plane without phase differential from the angled wavefield. Created with the scanning scheme shown in figure 23. Left: phase reconstruction. Right: intensity reconstruction

6 Integrating Differential Phase

The phase is extracted from the differential phase by using properties of the Fourier transform. [16,17] First the differential phase along one of the directions is multiplied by i to make the two phase directions orthogonal. Then taking the Fourier transform of the sum of the two differential phases:

$$\mathscr{F}\left(\frac{\partial\phi}{\partial x}+i\frac{\partial\phi}{\partial y}\right)=\iint\left(\frac{\partial\phi}{\partial x}+i\frac{\partial\phi}{\partial y}\right)\cdot\exp\left(-i2\pi\left(x\cdot x'+y\cdot y'\right)\right)dxdy \tag{75}$$

Can be integrated to the image phase by using the Fourier derivative theorem:

$$\left(\frac{\partial}{\partial x}+i\frac{\partial}{\partial y}\right)\phi=\left(\frac{\partial}{\partial x}+i\frac{\partial}{\partial y}\right)\mathscr{F}^{-1}\left(\mathscr{F}\left(\phi\right)\right) \tag{76}$$

$$\updownarrow$$

$$\frac{\partial\phi}{\partial x}+i\frac{\partial\phi}{\partial y}=\left(\frac{\partial}{\partial x}+i\frac{\partial}{\partial y}\right)\iint\mathscr{F}\left(\phi\right)\cdot\exp\left(i2\pi\left(x\cdot x'+y\cdot y'\right)\right)dx'dy' \tag{77}$$

Since $\mathscr{F}\left(\phi\right)$ is a function of only x' and y' then the differential operators only act on the exponential:

$$\frac{\partial\phi}{\partial x}+i\frac{\partial\phi}{\partial y}=\iint\mathscr{F}\left(\phi\right)\cdot\left(\frac{\partial}{\partial x}+i\frac{\partial}{\partial y}\right)\exp\left(i2\pi\left(x\cdot x'+y\cdot y'\right)\right)dx'dy' \tag{78}$$

$$\updownarrow$$

$$\frac{\partial \phi}{\partial x} + i\frac{\partial \phi}{\partial y} = \iint \mathscr{F}(\phi) \cdot i2\pi (x' + iy') \cdot \exp(i2\pi (x \cdot x' + y \cdot y'))\, dx'dy' \tag{79}$$

Taking the Fourier transform of both sides:

$$\mathscr{F}\left(\frac{\partial \phi}{\partial x} + i\frac{\partial \phi}{\partial y}\right) = \mathscr{F}(\phi)\, i2\pi (x' + iy') \tag{80}$$

$$\updownarrow$$

$$\mathscr{F}(\phi) = \frac{\mathscr{F}\left(\frac{\partial \phi}{\partial x} + i\frac{\partial \phi}{\partial y}\right)}{i2\pi (x' + iy')} \tag{81}$$

$$\updownarrow$$

$$\phi = \mathscr{F}^{-1}\left(\frac{\mathscr{F}\left(\frac{\partial \phi}{\partial x} + i\frac{\partial \phi}{\partial y}\right)}{i2\pi (x' + iy')}\right) \tag{82}$$

During the process the resolution of the output images can be set by padding or removing pixels. The two differential fields might not have a perfect solution and increasing the resolution of the result makes it possible to be more consistent with differentials in both directions. Restoring the differentials from more images taken at different lens positions does not increase the level of detail since the result is a least squares fit. Increasing the lens translation between images or the number of images means that the result is more noise resistant but the result contains more contributions from features outside the artificial aperture used during stitching.

6.1 Mirroring Fourier Space

The Fourier transform assumes periodic boundary conditions which means that it is assumed that the image repeats indefinitely. This is a problem when doing integration as the phase in one edge and the opposite is likely to be very different. Integrating the differential phase across this edge results in a solution which attempts to smooth the phase across the edge. The solution to this is creating a mosaic of four images by mirroring the image across the edges. By doing this the edges become identical. This new mosaic of four mirrored differential phase images has periodic boundaries and thus Equation 82 can be used to integrate the differential phase from such a image.

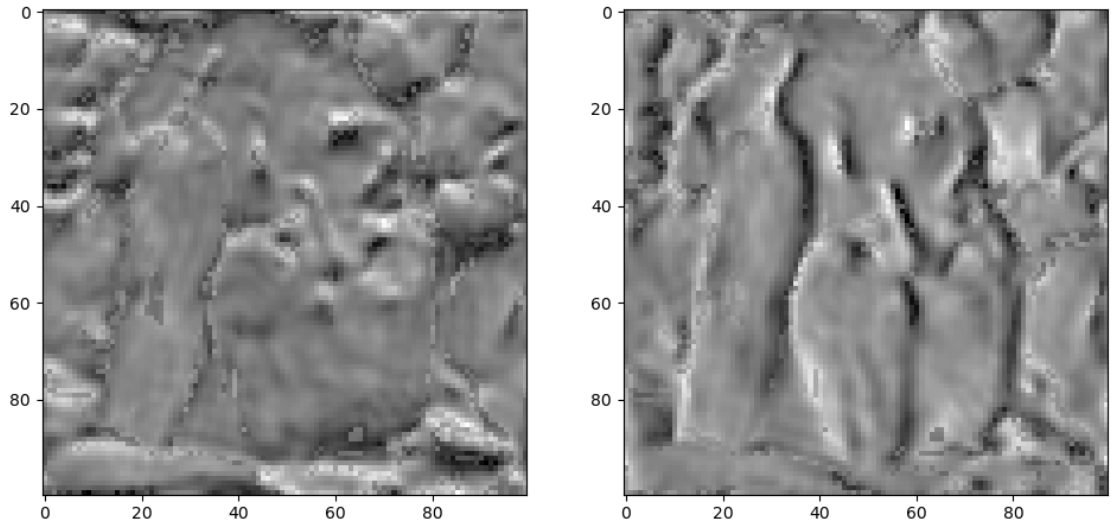

Figure 20: Left: example of differential phase along y. Right: example of differential phase along x.

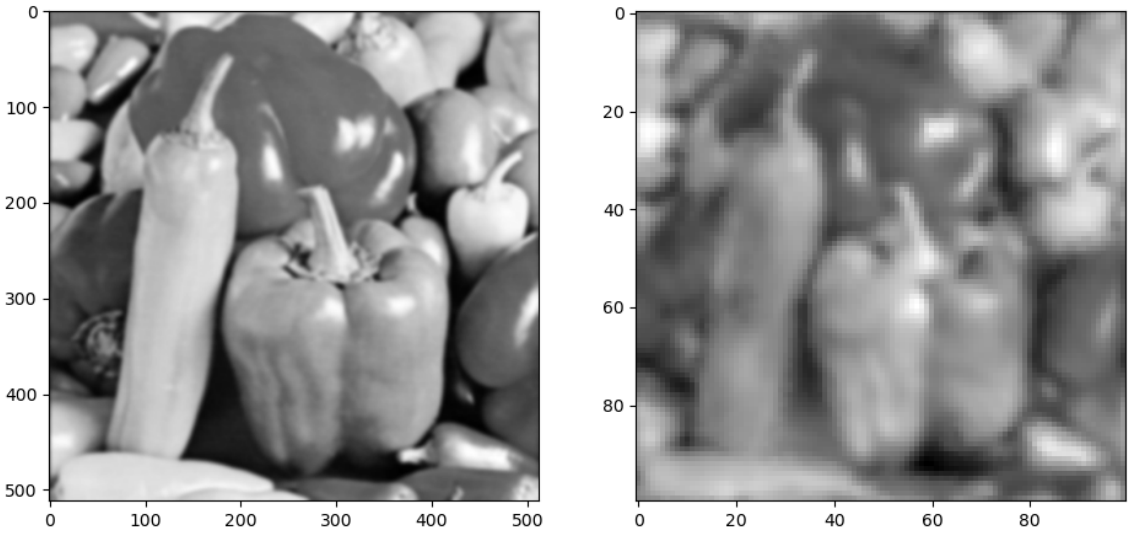

Figure 21: Left: Original. Right: Integrated from the differential phase images.

7 Stitching Phase

Integration of the deterministic phase gradients provides reconstructions of optical phase but the least squares fitting means that it is averaged over lens positions rather than combined. The deterministic phase gradients are assumed to be linear with lens translation. This assumption holds as long as the same details are captured by the Fourier components. Different features revealed by changing lens position cannot be assumed to be correlated with previously found features. The individual reconstructions are thus limited by the information contained in the wavefield passing trough the aperture. To achieve high resolution reconstruction a large area of the Fourier-plane must be determined. To do this wavefields from different phase gradients can be stitched together in what is essentially non-iterative or Deterministic Fourier Ptychography. Firstly a scanning scheme is used to capture images in groups at different lens positions. Each group is then reconstructed to phase gradients and then integrated to wavefields. These wavefields can now be back-propagated to the lens where the inverse transfer function is applied. The wavefields are then stitched into the Fourier-plane. There is no need to iterate over wavefields since they are assumed to be accurate representations of phase. The intensities can be determined as the mean of the group as the distance between members must be small such that the assumption of linear phase gradients remains true. The phase of the wavefields has an unknown phase offset since it originates from integration of differential phase. As with all other integration this leaves an unknown constant offset. The phase is aligned in the Fourier-plane by adding the mean phase offset to the part of the wavefield that should be included. The mean offset is calculated as the mean of a set of angles is calculated with complex numbers. First the overlapping area of the current wavefield and the new incoming wavefield needs to be found:

$$o = T \cap \psi_{\text{current}} \tag{83}$$

ψ_{current} is the current reconstruction and T is the transfer function of the next wavefield to be back-propagated from the detector-plane. Dividing the normalized wavefields is identical to subtracting the phases:

$$\psi_{\text{offset}}\left(\vec{r}\right) = \exp\left(i\left(\phi_{\text{back}}\left(\vec{r}\right) - \phi_{\text{current}}\left(\vec{r}\right)\right)\right) = \frac{\psi_{\text{back}}\left(\vec{r}\right)\left|\psi_{\text{current}}\left(\vec{r}\right)\right|}{\psi_{\text{current}}\left(\vec{r}\right)\left|\psi_{\text{back}}\left(\vec{r}\right)\right|} \text{ for } \vec{r} \in o \tag{84}$$

The mean of $\psi_{\text{offset}}\left(\vec{r}\right)$ is $\bar{\psi}_{\text{offset}}$; its phase is the mean phase offset and the magnitude describes to which degree the phase offsets are identical across the overlapping area o. Multiply the back-

propagated wavefield with the normalized mean offset to get the aligned wavefield:

$$\psi_{\text{aligned back}}(\vec{r}) = \psi_{\text{back}}(\vec{r}) \cdot \frac{\bar{\psi}_{\text{offset}}}{|\bar{\psi}_{\text{offset}}|} \tag{85}$$

The aligned wavefield is then stitched into the current reconstruction. This is done for all groups such that the entire wavefield in the Fourier-plane is restored. The only exception is the first group which serves as the initial phase in the Fourier-plane. The full wavefield in the Fourier-plane is then back-propagated to the sample plane but now it is not aligned with the phantoms optical phase. When using Fourier Ring Correlation the phase must be aligned with the original sample phase for the correlation to make sense. This is done exactly as the alignment of the phase in the Fourier-plane except the entire wavefield is compared at once:

$$\psi_{\text{offset}} = \frac{\psi_{\text{back}}(\vec{r})\,|\psi_{\text{sample}}(\vec{r})\,|}{\psi_{\text{sample}}(\vec{r})\,|\psi_{\text{back}}(\vec{r})\,|} \tag{86}$$

Multiply the reconstruction with the normalized mean offset to get the phase aligned:

$$\psi_{\text{aligned}} = \psi_{\text{back}} \cdot \frac{\bar{\psi}_{\text{offset}}}{|\bar{\psi}_{\text{offset}}|} \tag{87}$$

This step isn't needed in an experimental case unless it needs to be aligned with the phase from another method. It doesn't make sense to define a true sample phase as it would depend on the phase of the incident wavefield. There is also the effect that any offset between two points on the sample by $n \cdot 2\pi n \in N$ will make the optical phase of the two points indistinguishable.
Now the performance of the method can be determined by calculating the Fourier Ring Correlation between the aligned wavefield and the phantom used for simulation. Fourier Ring Correlation is defined for images and not wavefields so the intensity and optical phase are compared separately.

7.1 Scanning Schemes

An optimal scanning scheme attempts to maximize coverage of reconstructions in the Fourier-plane while having a well defined lens position for the result of each intermediate reconstruction. Lets call the images resulting in single intermediate reconstruction a group, as previously done. Maximizing coverage in the Fourier-plane involves spacing groups apart such that they cover as much space as possible while retaining some overlap. Within a group the result will have a well defined lens position if the lens translation between members is very small. But this setup is very noise sensitive, small changes in measured intensity will cause large changes in the reconstructed differential phase

thus amplifying noise. Figure 22 shows an example of this. A well defined lens position is preferred since the lens positions within a group must show the same features. This means a balance between a well defined lens position and noise sensitivity has to be found. A general scanning scheme can be defined but the optimal scheme will depend on the amount of noise in the experiment. Two scanning schemes are presented here, each has the same number of groups but the number of images in each group is varied. Figure 23 shows a scanning scheme with three images per group, this is the minimal amount to have non-collinear lens translation which is necessary to restore phase reliably in two dimensions. Figure 24 shows a scanning scheme with five images per group to see if the quality improves with more images. The number of groups and group centers are identical such that the coverage of the Fourier-plane is identical for both schemes. This means results only depend on the quality within groups. The results for the triangle scheme can be seen in figure 25 and figure 27 for the phase and intensity respectively. The results for the cross scheme can be seen in figure 29 and figure 31. The full Fourier Ring Correlations are shown below the reconstructions. When stitching in the Fourier-plane the overlap between wavefields, which is necessary to align phase, means that a choice can be made for which group to use. One solution is using an approach similar to Fourier Ptychography by defining a ratio of intermediate results to use. The approach used here is to start from small lens translation and then only stitch previously empty areas of the Fourier-plane. This means each area of the Fourier-plane aligned with the results at the smallest lens translation possible where noise should have less of an effect. Another approach would be to use mostly the center of each group as this should minimize lens aberrations which are likely to increase towards the edge of the lens. Another reconstruction done as a function of the number of groups can be seen in figure 33. The Fourier Ring Correlation for each of these results can be seen in figure 34.

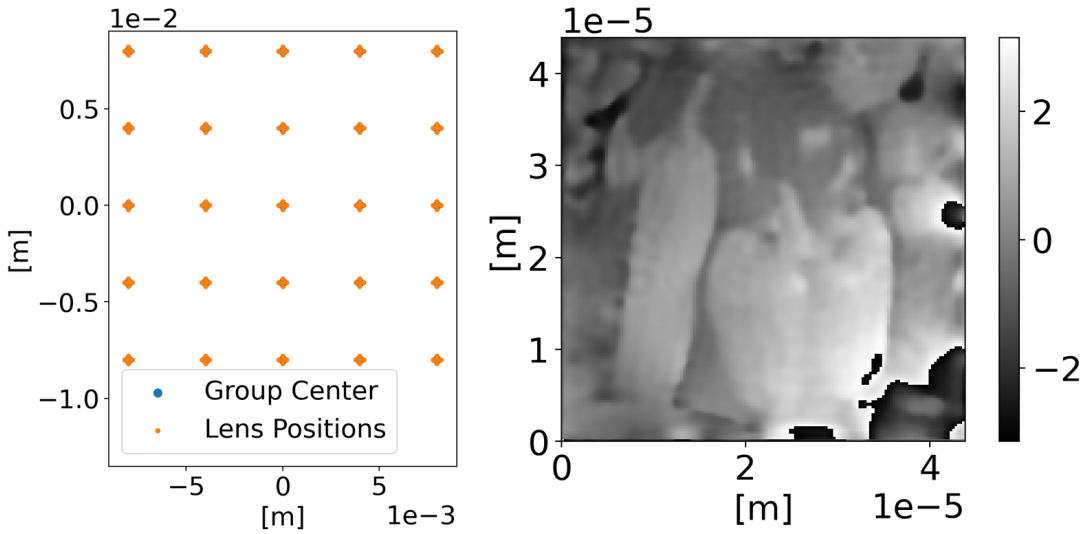

Figure 22: Left: Scanning scheme with very small distance between members of each group for a normal scanning scheme see figure 23 or figure 24. Since the results only contain numerical errors and errors from approximations the distance needs to be very small to show artifacts. Right: deterministic stitching result; there is a too high phase differential going from the top left to the bottom right.

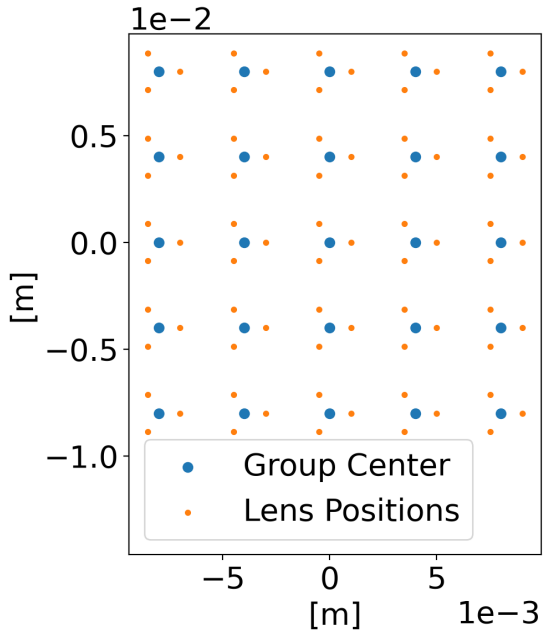

Figure 23: Lens centers in the Fourier-plane for the triangle scanning scheme with three images for each group. Coordinates show lens translation distance rather than frequency in Fourier space.

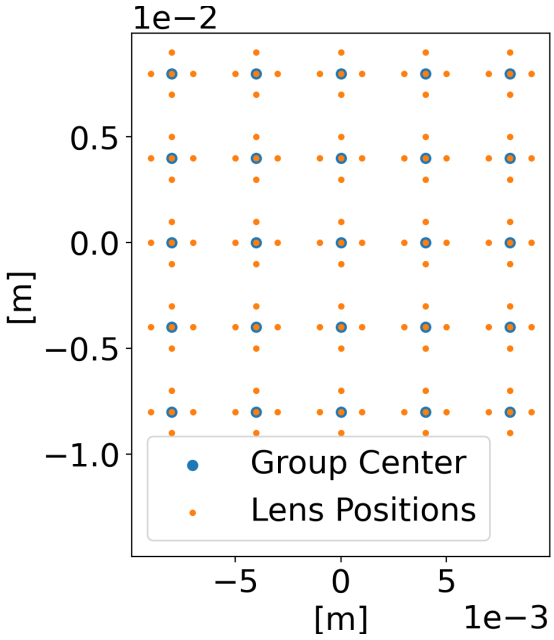

Figure 24: Lens centers in the Fourier-plane for the cross scanning scheme with five images for each group. Coordinates show lens translation distance rather than frequency in Fourier space.

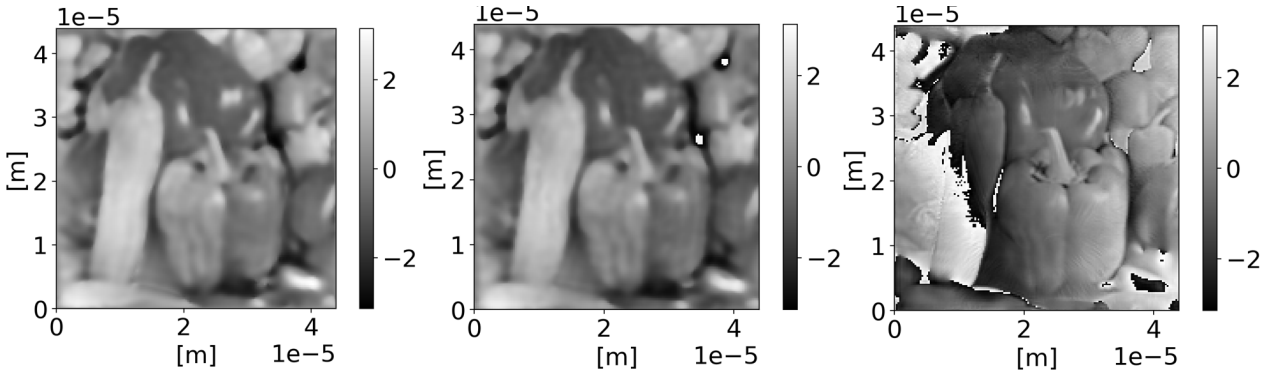

Figure 25: The results of reconstructing the phase with the scanning scheme in figure 23. The Fourier Ring Correlations (FRC) can be seen in figure 26. Left: Reconstruction using the central group and equation 72, resolution according to FRC: 0.649μm. Middle: Reconstruction using deterministic stitching on all groups, resolution according to FRC: 0.640μm. Right: Fourier Ptychography from all lens positions, resolution according to FRC: 14.7μm

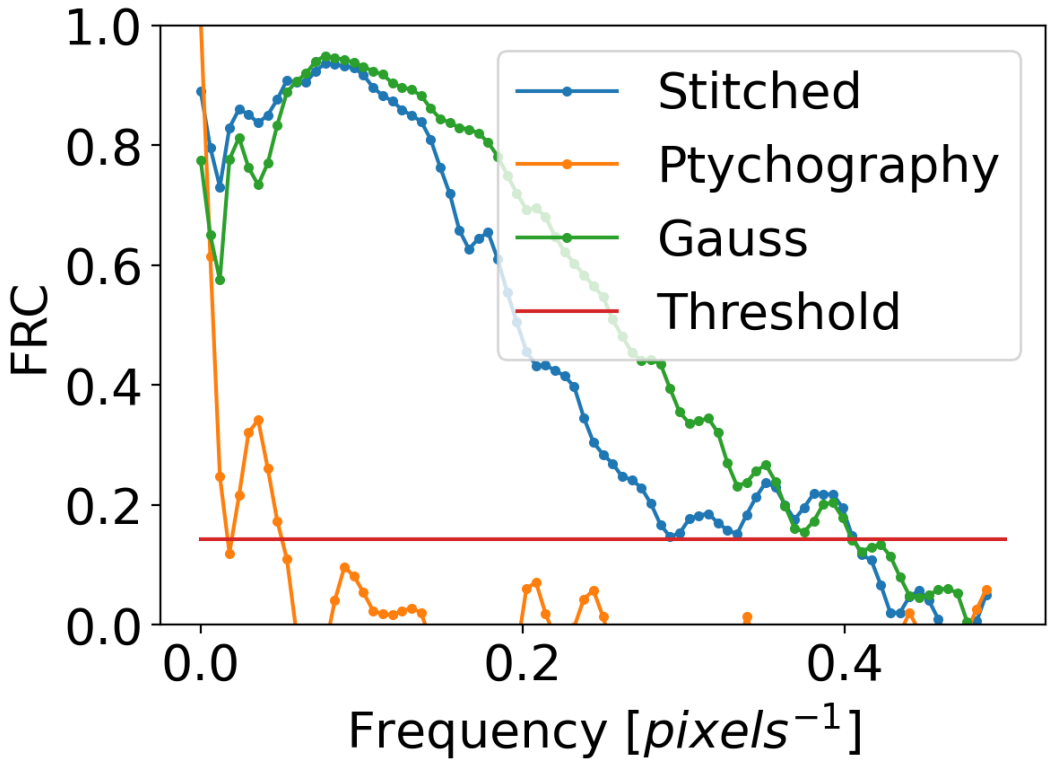

Figure 26: Fourier Ring Correlations of the results in figure 25 when compared with the original phantom. The threshold of $\frac{1}{7}$ is the minimum correlation for details to be defined as visible.

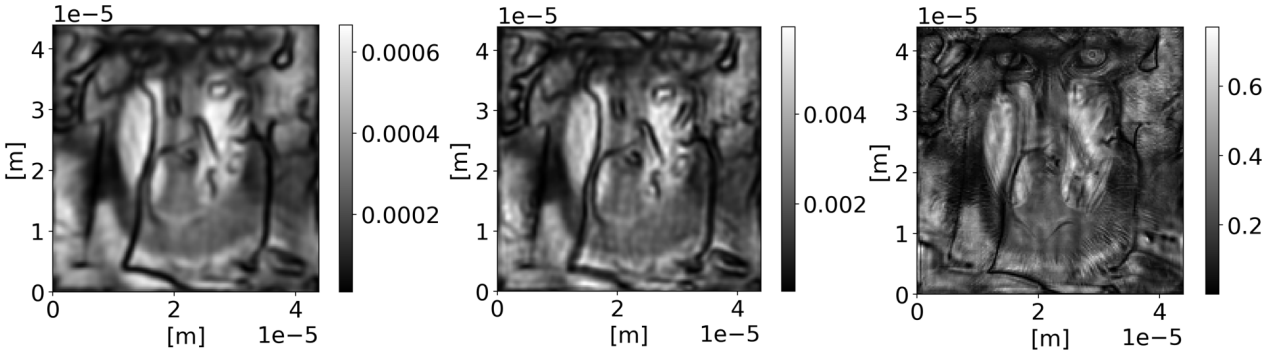

Figure 27: The results of reconstructing the intensity with the scanning scheme in figure 23. The Fourier Ring Correlations (FRC) can be seen in figure 28. Left: Reconstruction using the central group and equation 72, resolution according to FRC: $1.47\mu m$. Middle: Reconstruction using deterministic stitching on all groups, resolution according to FRC: $1.52\mu m$. Right: Fourier Ptychography from all lens positions, resolution according to FRC: $0.526\mu m$

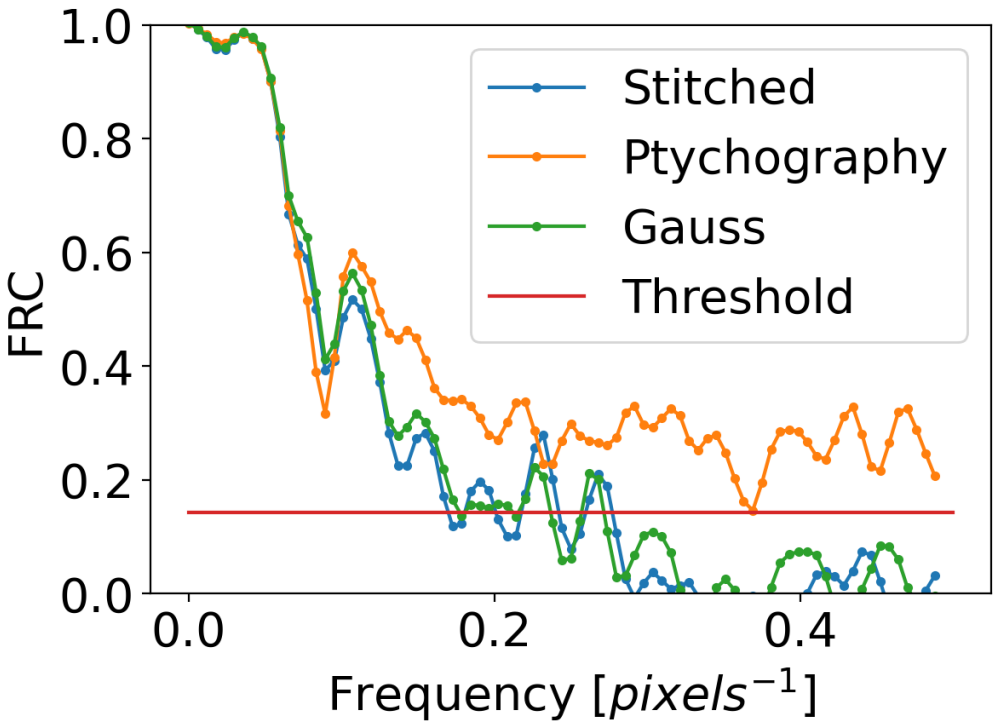

Figure 28: Fourier Ring Correlations of the results in figure 27 when compared with the original phantom. The threshold of $\frac{1}{7}$ is the minimum correlation for details to be defined as visible.

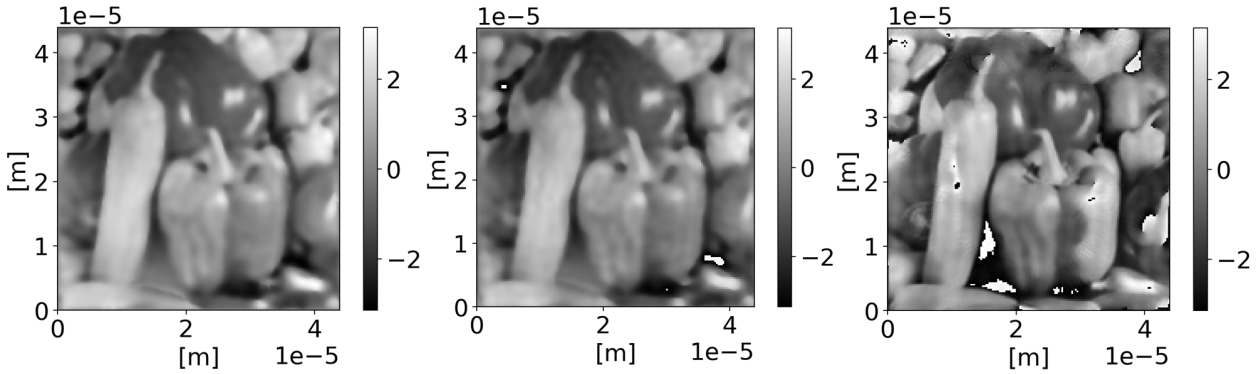

Figure 29: The results of reconstructing the phase with the scanning scheme in figure 24. The Fourier Ring Correlations (FRC) can be seen in figure 30. Left: Reconstruction using the central group and equation 72, resolution according to FRC: 0.605μm. Middle: Reconstruction using deterministic stitching on all groups, resolution according to FRC: 0.679μm. Right: Fourier Ptychography from all lens positions, resolution according to FRC: 0.526μm

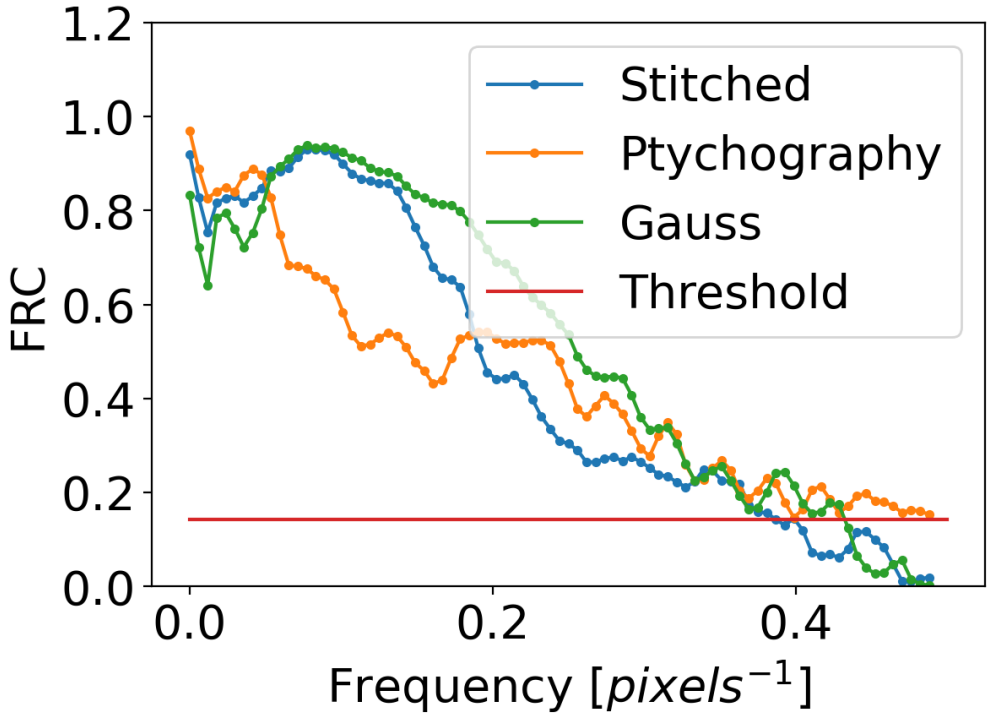

Figure 30: Fourier Ring Correlations of the results in figure 29 when compared with the original phantom. The threshold of $\frac{1}{7}$ is the minimum correlation for details to be defined as visible.

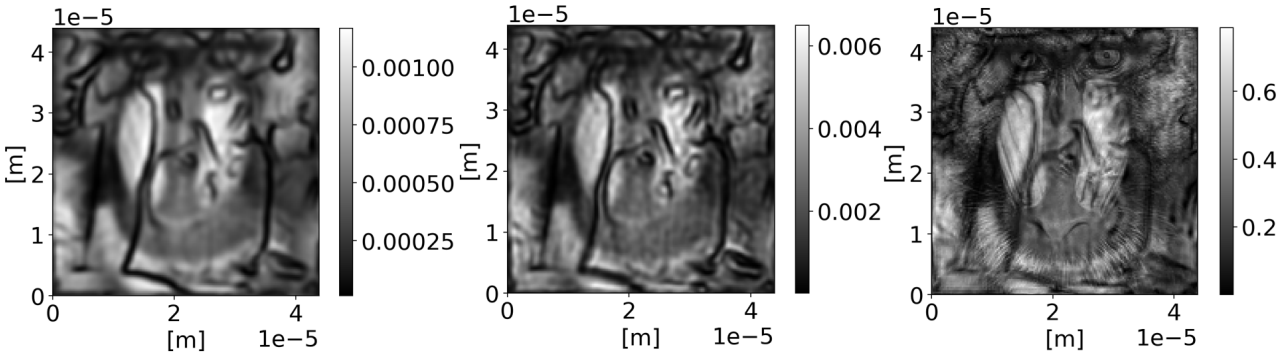

Figure 31: The results of reconstructing the intensity with the scanning scheme in figure 24. The Fourier Ring Correlations (FRC) can be seen in figure 32. Left: Reconstruction using the central group and equation 72, resolution according to FRC: 1.47μm. Middle: Reconstruction using deterministic stitching on all groups, resolution according to FRC: 1.52μm. Right: Fourier Ptychography from all lens positions, resolution according to FRC: 0.526μm

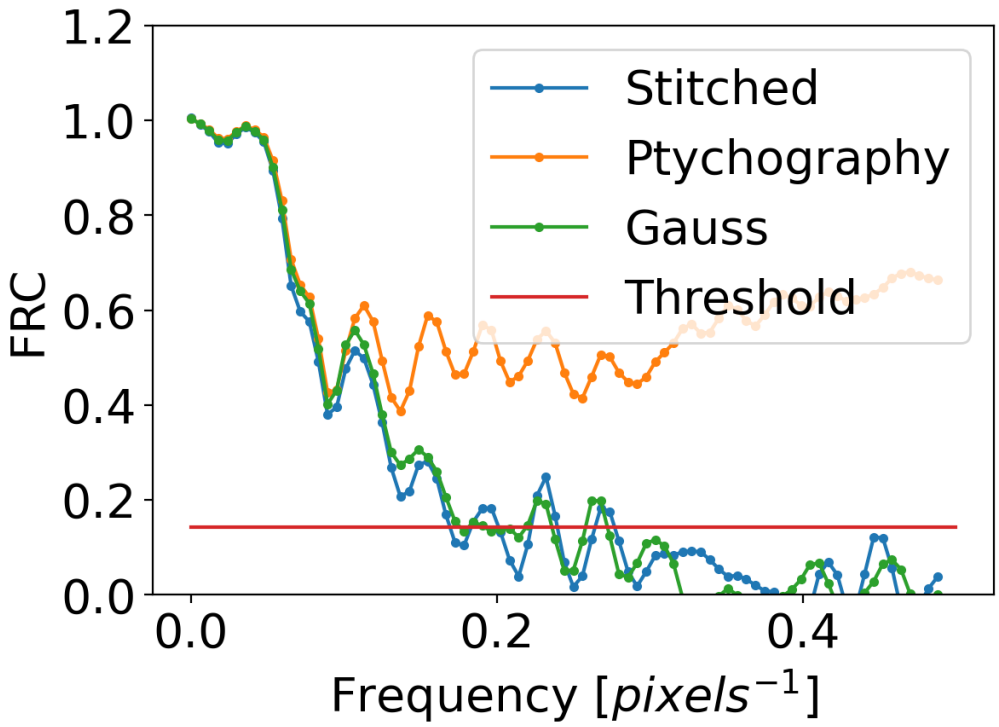

Figure 32: Fourier Ring Correlations of the results in figure 31 when compared with the original phantom. The threshold of $\frac{1}{7}$ is the minimum correlation for details to be defined as visible.

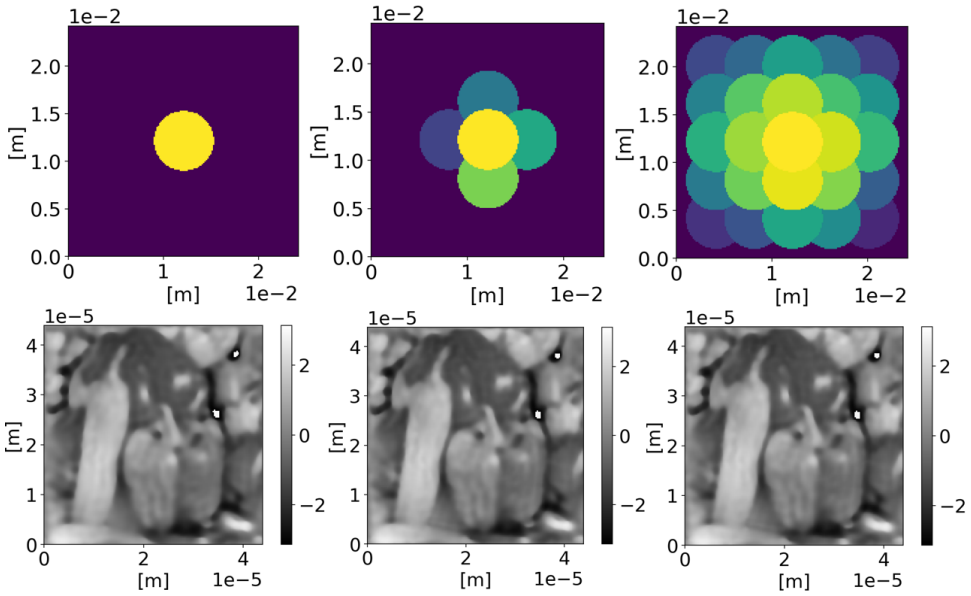

Figure 33: The top images show how the transmission functions cover the Fourier-plane, the color only serve to make them distinguishable. The bottom show the reconstructed phase. Left: back-propagation with just a single group, FRC: 1.30μm. Center: back-propagation after stitching 5 groups, FRC: 0.640μm. Right: back-propagation after stitching all 25 groups, FRC: 0.640μm

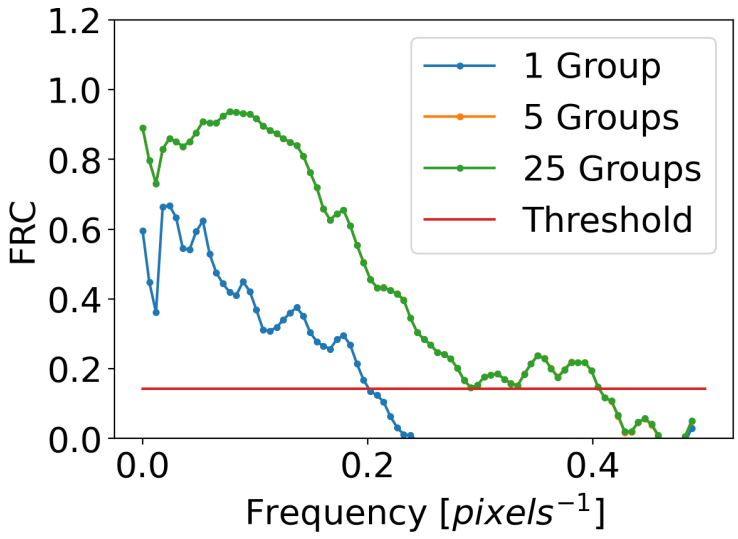

Figure 34: Fourier Ring Correlations of the reconstructions in figure 33. The FRC with 5 groups isn't visible as it is exactly covered by the datapoints of the FRC with 25 groups. This shows that there is no improvement after the first five groups.

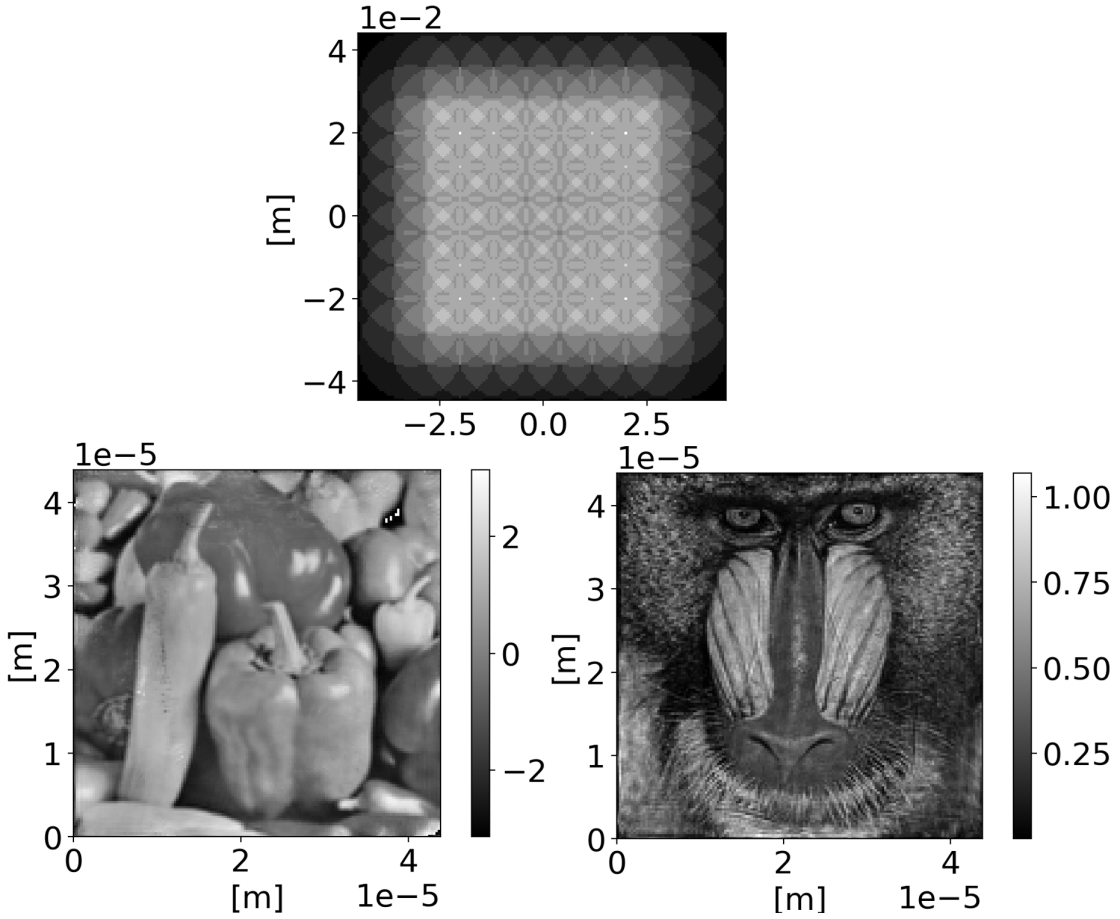

Figure 35: Fourier Ptychography results when using a regular scanning lens translation scheme with 81 measured images and without a Gaussian apodizer. Top: Coverage of the Fourier-plane when using the scanning scheme. Left: Phase reconstruction after 10 iterations. Right: Intensity reconstruction after 10 iterations. The pixel size of the reconstructions is $0.574\mu m$, the resolution given by the Fourier Ring Correlation in figure 36 is $1.15\mu m$.

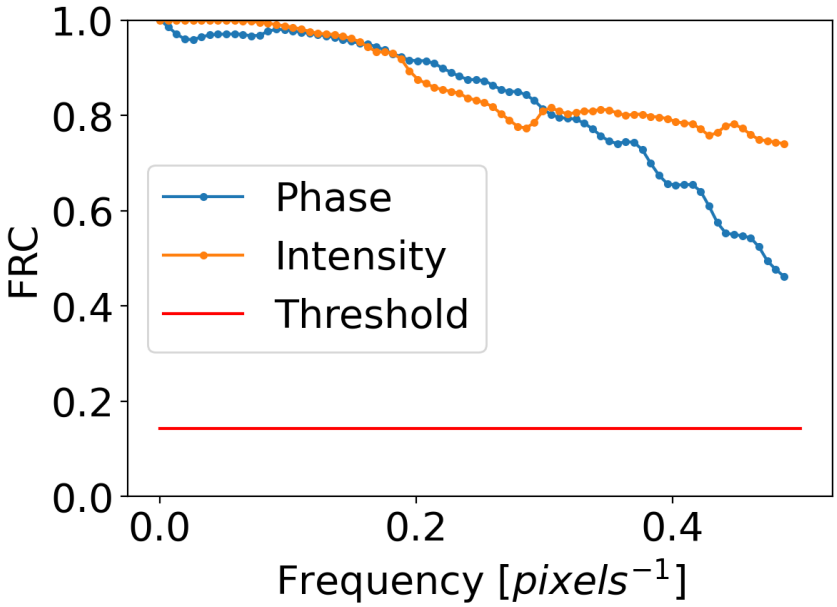

Figure 36: Fourier Ring Correlation of the phase and intensity in figure 35 when compared with the originals in figure 6. Since the Fourier Ring Correlation doesn't go below $\frac{1}{7}$ the resolution is the maximum possible, which is 2 pixels ($1.15\mu m$).

8 Discussion

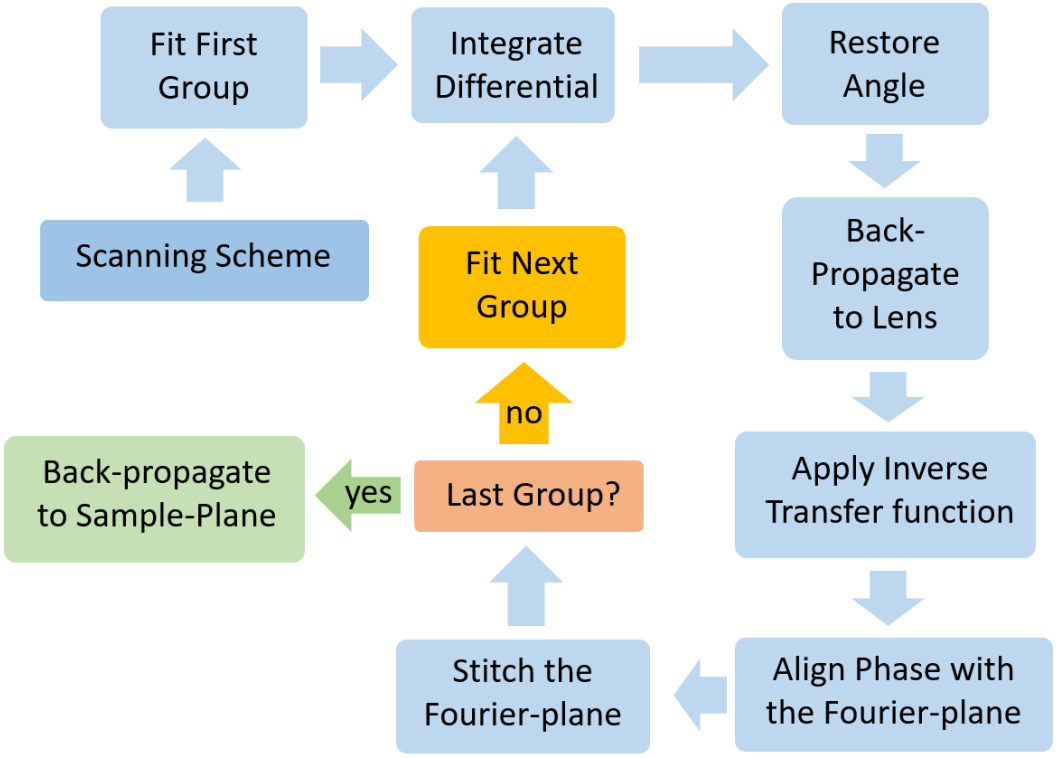

Figure 37

First a recap and overview of Deterministic Fourier Ptychography, also see the flowchart in figure 37:

1. Images are measured in groups according to a scanning scheme like figure 23 or 24.
2. A group is reconstructed by using Tikhonov regularization to solve equation 72 for the differential phase in 2 dimensions.
3. The wavefield of the group is restored by integrating the mirrored differential phase using equation 82. The amplitude in each pixel is set to the square-root of the mean measured intensity in that pixel.
4. The forward simulated differential phase corresponding to the lens position of the group center is added to the wavefield according to equation 74.

5. The wavefield is back-propagated to the lens-plane and the inverse transfer function is applied, as in Fourier Ptychography.

6. The wavefield is aligned with the Fourier-plane by comparing overlapping areas as in equation 84 and 85.

7. The wavefield is stitched into the empty portion of the Fourier-plane, as shown in figure 33.

8. Repeat from 2. until all groups have been stitched into the Fourier-plane.

9. The full wavefield in the Fourier-plane is back-propagated to the sample-plane thus creating a reconstruction of sample properties.

Deterministic stitching has one known major problem which remains to be solved; the restoration of beam angles by forward simulation without a sample doesn't work for dark-field images at all. No intensity reaches the detector if there is no sample, by the definition of dark-field images. The assumption that the contribution can be isolated from the sample contribution to the wavefield should be true for this to work, even when forward simulation is possible. If the solution depends on sample properties then it becomes even harder if not impossible to solve deterministically since these properties must be derived from the wavefield in the detector-plane. The problem might need to be solved analytically to get the correct differential phase contribution for all possible illumination angles. Another solution would be to attempt to remove the artifacts which arise when stitching without aligning any angles, as shown in figure 19.
It has been decided to limit the project here, there is no proof whether more problems arise before dark-field images can be successfully stitched.
Given the current progress Deterministic Fourier Ptychography generally performs worse than normal Fourier Ptychography. This is contrary to what Fourier Ring Correlation shows for the phase reconstructions in figure 26 and figure 30. This rather shows a disadvantage of using Fourier Ring Correlation for phase contrast images. The correlation is low if the phase in a reconstruction changes by more than 2π while the phantoms optical phase doesn't. The Fourier Ring Correlation doesn't account for the periodic phase and thus penalizes a change from $-\pi$ to π even if it remains close to the optical phase of the phantom. In this case the reconstructed intensities are much better for describing the quality of the reconstructions. Fourier Ptychography performs better in these cases as can be seen in figure 28 and figure 32.

Deterministic Fourier Ptychography has fewer artifacts in the phase reconstruction when compared to Fourier Ptychography but this might be related to the higher level of detail of Fourier Ptychography. Fourier Ptychography usually uses a equally spaced scanning scheme without a Gaussian apodizer, this is done in figure 35 and results in an even better correlation as can be seen in figure 36. It has the advantage that as long as an accurate simulation of aberrations and propagation is used then the result should converge. The simulation used to create the measurements is in this case identical to the methods for reconstructing the sample. This means the reconstructions should be good since some of the steps are a perfect match to how the images were created.

The underlying problem for Deterministic Fourier Ptychography is that it requires very precise calculation of each step to reach a successful reconstruction. Since there is no iterative error reduction the solution to every step must be very accurate.

The reconstruction quality hardly changes between the two scanning schemes tested here, figure 23 and 24. Only Fourier Ptychography improves considerably with the extra measurements; both phase and intensity has better FRC with the extra images in the cross scanning scheme. This shows that, with the parameters used here, nothing is gained for the deterministic methods by using more than 3 images for each group. This again highlights that stitching is necessary to increase the resolution further.

Figure 34 shows that the resolution increases when the first few intermediate reconstructions are stitched together. This shows that the stitching must work somewhat. The changes are however small enough to not be visible by looking at the reconstructions. As can be seen in figure 33 the last groups are at larger tilt and that they don't improve resolution is likely linked to the missing differential phase contribution for dark-field images.

The effect of forward simulating the angle doesn't affect the Gaussian reconstruction method much for bright-field images. This shows as the reconstruction method with the Gaussian apodizer even seems to allow for resolution beyond the resolving power of the lens. The Abbe diffraction limit of the simulated setup is $1.07\mu m$ but Fourier Ring Correlation states resolutions around $0.6\mu m$ for the phase reconstructions. The method does a fit to data which is assumed to come from the same features and it should thus also be limited by the lens. The integration of differential phase in two dimensions might be the reason as it uses two differential values for each pixel. Another probable reason is that the sample doesn't contain a number of well defined features just below the resolution reached and thus the Fourier Ring Correlation is high until a limiting number of features are gone.

Both of these reasons explain why the transmission reconstruction is worse as it isn't integrated and the phantom contains finer detail. From the Fourier Ring Correlations it can be seen that a single group of images reconstructed with the Gaussian apodizer performs just as well if not better than attempting to stitch several groups together.

9 Conclusion

The use of tilt aberration has been generalized to arbitrary combinations of either lens positions or source angles. It had to be recalculated with a Gaussian apodizer to avoid bias when not using tilt measurements centered at zero. The reconstructed differential phase has been integrated to phase that can then be back-propagated to the Fourier-plane. A full simulation and reconstruction pipeline was programmed to compare performance under controlled conditions. The results show that the level of detail achieved during the stitching of Deterministic Fourier Ptychography still needs more work. The resolution is limited since the dark-field images aren't stitched correctly. This likely stems from the attempt at restoring the phase differential from the beam angle by forward simulation which doesn't work for dark-field images.

Some conclusions on the usefulness of the method can be made regardless of this. The method requires computations that could slow it down, this is likely to limit if not entirely remove the speed advantage it had over Fourier Ptychography. The computations needed beyond the ones in Fourier Ptychography are: reconstruction in the detector plane, aligning beam angles and integration. Whether this takes longer likely depends on the number of iterations needed for Fourier Ptychography to reach the same result.

While the deterministic results generally have fewer artifacts than Fourier Ptychography it is not enough to conclude that it is less noise sensitive as it has a too low level of detail to be comparable. There is nothing which suggests that it is more or less sensitive to noise or misalignment of the experimental setup. Noise in both methods will manifest as errors in the differential phase which will affect the entire image. The error reduction of Tikhonov regularization helps here and since it also compares multiple images it is likely to perform as well as the iterative error reduction of Fourier ptychography.

Something of special interest is that the use of a Gaussian transmission function from a Gaussian apodizer allows for fast deterministic reconstructions of phase in the detector-plane. It could

potentially be an improvement to Differential Phase Contrast. It could likely also be used to create initial guesses for Fourier Ptychography, whether it is a considerable improvement is not known. For future progress on Deterministic Fourier Ptychography the differential phase in the detector-plane as a function of illumination angle needs to be investigated further. If the results get to be on par with Fourier Ptychography it could be of interest to see if some of the steps could be done differently to improve computation time or improve performance.

10 References

[1] P. C. Konda et al. "Fourier ptychography: current applications and future promises." *Optics Express*, 2020, **28**(7), 9603-9630.

[2] R. Horstmeyer et al. "Digital pathology with Fourier ptychography." *Computerized medical imaging and graphics*, 2014, **42**, 38-43.

[3] L. Tian et al. "Computational illumination for high-speed in vitro Fourier ptychographic microscopy." *Optica*, 2015, **2**(10), 904-911.

[4] C. Guo et al. "OpenWSI: a low-cost, high-throughput whole slide imaging system via single-frame autofocusing and open-source hardware." *Optics Letters*, 2020, **45**(1), 260-263.

[5] S. Dong et al. "FPscope: a field-portable high-resolution microscope using a cellphone lens." *Biomedical optics express*, 2014, **5**(10), 3305-3310.

[6] H. Simons et al. "X-ray Fourier ptychographic microscopy." *arXiv* preprint, 2016, arXiv:1609.07513.

[7] K. Wakonig et al. "X-ray Fourier ptychography." *Science advances*, 2019, **5**(2), eaav0282.

[8] J. Als-Nielsen and D. McMorrow, *Elements of Modern X-ray Physics*, John Wiley & Sons Ltd, Chichester, 2011.

[9] C. Detlefs et al. "Translative lens-based full field coherent X-ray imaging." *Journal of synchrotron radiation*, 2020, **27**(1): 119-126

[10] D. M. Paganin, *Coherent X-ray optics*, Oxford University Press, 2006.

[11] A. M. Maiden and J. M. Rodenburg, "An improved ptychographical phase retrieval algorithm for diffractive imaging." *Ultramicroscopy*, 2009, **109**(10), 1256-1262.

[12] R. P. J. Nieuwenhuizen et al. "Measuring image resolution in optical nanoscopy." *Nature Methods*, 2013, **10**(6), 557-562.

[13] J. B. Pendry, "Negative Refraction Makes a Perfect Lens." *Physical Review Letters*, 2000, **85**(18), 3966-3969.

[14] X. Zhang and Z. Liu "Superlenses to overcome the diffraction limit." *Nature Materials*, 2008, **7**(6), 435-441.

[15] L. Tian, and L. Waller, "Quantitative differential phase contrast imaging in an LED array microscope." *Optics express*, 2015, **23**(9), 11394-11403.

[16] C. Kottler et al. "A two-directional approach for grating based differential phase contrast imaging using hard x-rays." *Optics express*, 2007, **15**(3), 1175-1181.

[17] K. S. Morgan et al. "X-ray phase imaging with a paper analyzer." *Applied Physics Letters*, 2012, **100**(12), 124102.

[18] J. Sun et al. "Single-shot quantitative phase microscopy based on color-multiplexed Fourier ptychography." *Optics Letters*, 2018, **43**(14), 3365-3368.

[19] Z. Guoan et al. "Wide-field, high-resolution Fourier ptychographic microscopy." *Nature Photonics*, 2013, **7**(9), 739.

[20] S. B. Mehta and C. J. R. Sheppard, "Quantitative phase-gradient imaging at high resolution with asymmetric illumination-based differential phase contrast." *Optics Letters*, 2009, **34**(13), 1924-1926.

[21] D. Paganin, T. Petersen and M. Beltran, "Propagation of fully-coherent and partially-coherent complex scalar fields in aberration space." *Phys. Rev. A*, 2018, **97**, 023835.

11 Appendix

Tilt aberration arises through a series of different equations, principles and approximations. A derivation of tilt aberration shows the validity in using the theory and the limitations due to the approximations used.

11.1 Scalar Diffraction Theory

The derivation will begin from Scalar Diffraction theory since this can be derived from the vacuum field equations which in turn can be derived from the free space Maxwell equations [1]. Scalar Diffraction theory describes a electromagnetic wave by a single complex scalar function which is a function of spatial coordinates and time. Scalar diffraction theory has the limitation that all components of the wave must abide by the same wave equation. This means the theory doesn't handle interactions which affect individual spatial components of the electric or magnetic field or if the interactions couple these components. The theory is therefore not suited for changes in the permittivity or boundary conditions on the scale of a few wavelengths however the error will be small if the features are large compared to the wavelength. [2]
The core of scalar diffraction theory is the Helmholtz equation:

$$\left(\nabla^2 + k^2\right) \psi_\omega \left(\vec{r}, t\right) = 0 \tag{88}$$

Which can be rewritten as:

$$\nabla^2 \psi_\omega \left(\vec{r}, t\right) = -k^2 \psi_\omega \left(\vec{r}, t\right) \tag{89}$$

Where k is the wavenumber given by: $k = \frac{\omega}{c}$ and $\vec{r}$ is a vector of the Cartesian spatial coordinates:

$$\vec{r} = \begin{bmatrix} x \\ y \\ z \end{bmatrix} \tag{90}$$

One solution to the Helmholtz equation is the plane harmonic wave given by:

$$\psi_\omega \left(\vec{r}, \vec{k}, t\right) = A \cdot e^{i\left(\vec{r}\cdot\vec{k} \pm \omega t\right)} \tag{91}$$

Where $\vec{k}$ is the wavevector describing the direction of the plane wave:

$$\vec{k} = \begin{bmatrix} k_x \\ k_y \\ k_z \end{bmatrix} \tag{92}$$

$$|\vec{k}| = k = \sqrt{{k_x}^2 + {k_y}^2 + {k_z}^2} = \frac{\omega}{c} = \frac{2\pi}{\lambda} \tag{93}$$

Another solution is the harmonic spherical wave:

$$\psi_\omega(r,t) = \frac{A}{r} \cdot e^{i(r\cdot k \pm \omega t)} \tag{94}$$

Where r is the distance from the origin of the spherical wave. Differentiating either of these solutions twice with respect to time gives:

$$\frac{\partial^2 \psi}{\partial t^2} = -\omega^2 \psi \tag{95}$$

Using $\omega = kc$ from eq. 93:

$$\frac{\partial^2 \psi}{\partial t^2} = -k^2 c^2 \psi \tag{96}$$

$$\updownarrow$$

$$\frac{1}{c^2}\frac{\partial^2 \psi}{\partial t^2} = -k^2 \psi \tag{97}$$

Finally by substituting using eq. 89 the differential wave equation is derived:

$$\nabla^2 \psi_\omega(\vec{r},t) = \frac{1}{c^2}\frac{\partial^2 \psi}{\partial t^2} \tag{98}$$

11.2 Huygens-Fresnel Principle

The goal of this section is showing how Huygens-Fresnel principle can be used to determine the wavefunction at an arbitrary point within a volume given that the wavefunction is known along the entire edge of the volume. To make it similar to a instrumental setup with an aperture the incoming field is assumed to only pass through a plane at the edge of the volume as seen on figure 38. The Huygens-Fresnel principle can be derived from the differential wave equation by using Green's functions. Green's second identity is given by:

$$\iint_s ds \left(U\frac{\partial G}{\partial N} - G\frac{\partial U}{\partial N} \right) = \iiint_V dV \left(G\nabla^2 U - U\nabla^2 G \right) \tag{99}$$

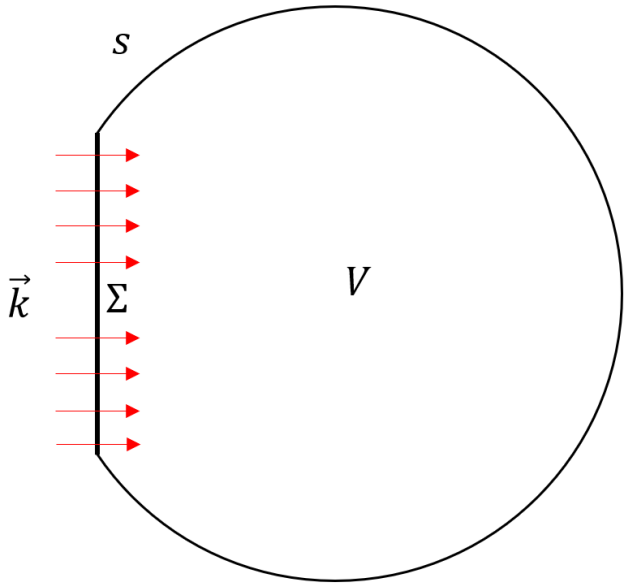

Figure 38: The volume V with the surface s. Σ is the subset of the surface for which the incoming wave is non-zero.

s is a surface enclosing volume V and $\iint_s ds$ is the integral across this surface. $\frac{\partial}{\partial N}$ is differentiation along the normal with respect to s. Intuitively Green's second identity says that if the value and first differential of two functions is known along a surface then the values can be determined in the enclosed volume.

Setting $U = \psi$ and assuming that ψ and G are solutions to both the Helmholtz equation and the Differential wave equation:[3]

$$\iint_s ds \left(\psi \frac{\partial G}{\partial N} - G \frac{\partial \psi}{\partial N}\right) = \iiint_V dV \left(G \frac{1}{c^2} \frac{\partial^2 \psi}{\partial t^2} - \psi \frac{1}{c^2} \frac{\partial^2 G}{\partial t^2}\right) \tag{100}$$

Substituting by using eq. 96:

$$\iint_s ds \left(\psi \frac{\partial G}{\partial N} - G \frac{\partial \psi}{\partial N}\right) = \iiint_V dV \left(-G \frac{1}{c^2} k^2 c^2 \psi + \psi \frac{1}{c^2} k^2 c^2 G\right) \tag{101}$$

$$\updownarrow$$

$$\iint_s ds \left(\psi \frac{\partial G}{\partial N} - G \frac{\partial \psi}{\partial N}\right) = 0 \tag{102}$$

G is set to the sum of two free space Green's functions mirrored by the plane of incoming rays in s, as done by Sommerfeld[2]. The Green's function at a point P is given by:[2,3]

$$G(\vec{P}) = \frac{\exp(ikr)}{r} - \frac{\exp(ikr_-)}{r_-} \tag{103}$$

And the derivative of G with respect to the normal of s:

$$\frac{\partial G}{\partial N} = \cos(\theta)\left(\frac{ik\exp(ikr)}{r} - \frac{\exp(ikr)}{r^2}\right) - \cos(\theta_-)\left(\frac{ik\exp(ikr_-)}{r_-} - \frac{\exp(ikr_-)}{{r_-}^2}\right) \tag{104}$$

Where r is the distance from some initial point P_0 inside the volume to the point P. r_- is the distance from the mirrored point P_{0-} to P. θ is the angle between a vector from P_0 to P and the normal of s. θ_- is the angle between a vector from P_{0-} to P and the normal of s.
Since the function used in Green's theorem must have a continuous first and second derivative then the singularity at $r = 0$ is excluded from the volume V by containing the point P_0 in a small spherical volume with radius ϵ, see figure 39. Therefore the surface of integration is now:

$$s = s' + s_\epsilon \tag{105}$$

Integration across the surface s can thus be split into the sum of the integration across s' and s_ϵ:

$$\iint_s ds\left(\psi\frac{\partial G}{\partial N} - G\frac{\partial \psi}{\partial N}\right) = \iint_{s'} ds\left(\psi\frac{\partial G}{\partial N} - G\frac{\partial \psi}{\partial N}\right) + \iint_{s_\epsilon} ds\left(\psi\frac{\partial G}{\partial N} - G\frac{\partial \psi}{\partial N}\right) = 0 \tag{106}$$

The integral over s_ϵ can be calculated by letting ϵ become infinitesimally small as from eq. 103 and eq. 104 the value of G and its derivative along the normal of s_ϵ at all points on s_ϵ can be determined:

$$\lim_{\epsilon\to 0} G(s_\epsilon) = \lim_{\epsilon\to 0}\left(\frac{\exp(ik\epsilon)}{\epsilon} - \frac{\exp(ik(r_-))}{r_-}\right) \tag{107}$$

$$\lim_{\epsilon\to 0}\frac{\partial G(s_\epsilon)}{\partial N} = \lim_{\epsilon\to 0}\left(-\left(\frac{ik\exp(ik\epsilon)}{\epsilon} - \frac{\exp(ik\epsilon)}{\epsilon^2}\right) - \cos(\theta_-)\left(\frac{-ik\exp(ikr_-)}{r_-} + \frac{\exp(ikr_-)}{{r_-}^2}\right)\right) \tag{108}$$

Only keeping terms of lowest order in ϵ:

$$\lim_{\epsilon\to 0} G(s_\epsilon) = \lim_{\epsilon\to 0}\frac{\exp(ik\epsilon)}{\epsilon} \tag{109}$$

$$\lim_{\epsilon\to 0}\frac{\partial G(s_\epsilon)}{\partial N} = \lim_{\epsilon\to 0}\frac{\exp(ik\epsilon)}{\epsilon^2} \tag{110}$$

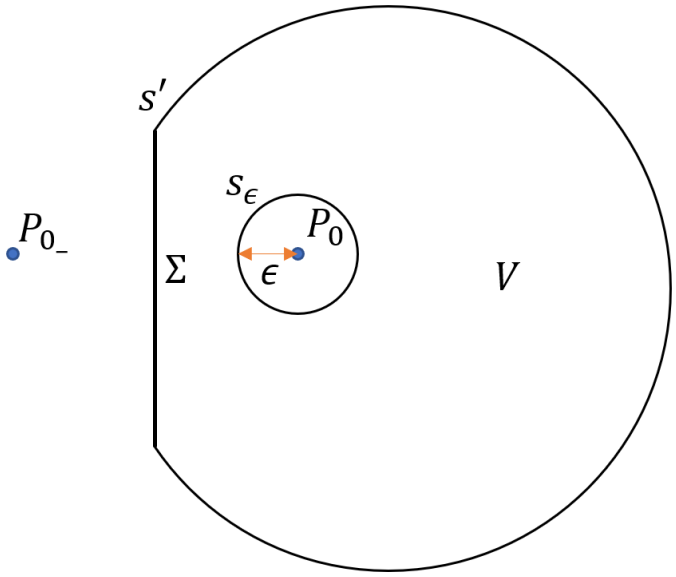

Figure 39: $P_{0\_}$ is P_0 mirrored in Σ which is a subset of s'. The point P_0 is excluded from the volume by the spherical surface s_ϵ with radius ϵ.

Noting here that the cosine from the first term has been removed since it is always minus one as the angle, θ, between the vector from P_0 to P and the normal of the surface s_ϵ is 180°.
When epsilon goes towards zero the value of ψ and G approaches a constant which is their value at P_0. Since the value in the integral becomes constant the integral can be exchanged with multiplication by the area of a sphere with radius ϵ:

$$\lim_{\epsilon\to 0}\iint_{s_\epsilon} ds\left(\psi\frac{\partial G}{\partial N}-G\frac{\partial\psi}{\partial N}\right)=\lim_{\epsilon\to 0}4\pi\epsilon^2\left(\psi(P_0)\frac{\partial G}{\partial N}-G\frac{\partial\psi(P_0)}{\partial N}\right) \tag{111}$$

$$\updownarrow$$

$$\lim_{\epsilon\to 0}\iint_{s_\epsilon} ds\left(\psi\frac{\partial G}{\partial N}-G\frac{\partial\psi}{\partial N}\right)=\lim_{\epsilon\to 0}4\pi\epsilon^2\left(\psi(P_0)\frac{\exp(ik\epsilon)}{\epsilon^2}-\frac{\exp(ik\epsilon)}{\epsilon}\frac{\partial\psi(P_0)}{\partial N}\right) \tag{112}$$

$$\downarrow$$

$$\lim_{\epsilon\to 0}\iint_{s_\epsilon} ds\left(\psi\frac{\partial G}{\partial N}-G\frac{\partial\psi}{\partial N}\right)=4\pi\psi(P_0) \tag{113}$$

Inserting into eq. 106:

$$\iint_{s'} ds\left(\psi\frac{\partial G}{\partial N}-G\frac{\partial\psi}{\partial N}\right)+4\pi\psi(P_0)=0 \tag{114}$$

$$\updownarrow$$

$$\frac{1}{4\pi}\iint_{s'} ds\left(-\psi\frac{\partial G}{\partial N}+G\frac{\partial\psi}{\partial N}\right)=\psi(P_0) \tag{115}$$

There is no contribution from the area of s' for which there is no incoming waves. It is possible to show this using the Sommerfeld radiation condition. For this s' is assumed to be a sphere with

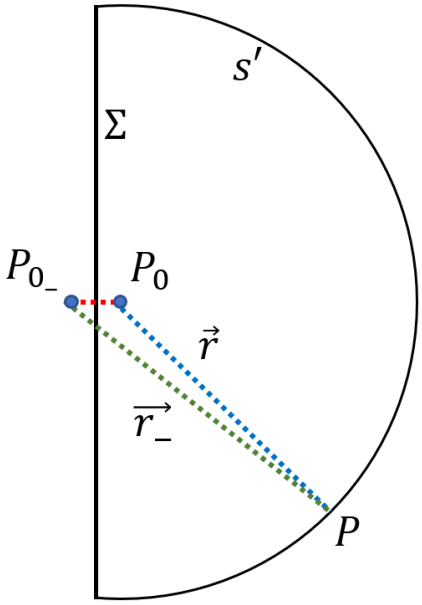

Figure 40: Illustration of how the angle between $\vec{r_-}$ and $\vec{r}$ approaches 0 when $|\vec{r}|$ approaches ∞.

radius $|\vec{r}|$ and center in P_0; see figure 40. Using trigonometry the angle between $\vec{r}$ and $\vec{r_-}$ can be determined as a function of the distances:

$$\cos(\theta-\theta_-)=\frac{|\vec{r}|+|\vec{r}+(\vec{p_0}-\vec{p_{0-}})\,|-|\vec{p_0}-\vec{p_{0-}}|}{2|\vec{r}||\vec{r}+(\vec{p_0}-\vec{p_{0-}})\,|} \tag{116}$$

The angles ϕ and ϕ_- are defined as in eq. 104 and $(\vec{p_0}-\vec{p_{0-}})$ is the vector between P_0 and P_{0-}. By taking the limit for the radius $|\vec{r}|$ going to infinity the contribution from $(\vec{p_0}-\vec{p_{0-}})$ disappears:

$$\lim_{|\vec{r}|\to\infty}\cos(\theta-\theta_-)=\lim_{|\vec{r}|\to\infty}\frac{|\vec{r}|+|\vec{r}|}{2|\vec{r}||\vec{r}|} \tag{117}$$

$$\updownarrow$$

$$\lim_{|\vec{r}|\to\infty}\cos(\theta-\theta_-)=\lim_{|\vec{r}|\to\infty}\frac{1}{|\vec{r}|} \tag{118}$$

$$\updownarrow$$

$$\lim_{|\vec{r}|\to\infty} \cos(\theta - \theta_-) = 0 \tag{119}$$

The possible values for $\theta - \theta_-$ is $\{n\pi | n \in Z\}$ where Z is the set of all integers. This can be further reduced to $\{2n\pi | n \in Z\}$ as P_{0-} is on the same side of s' as P_0.

θ is known to be 0 since θ was defined as the angle between $\vec{r}$ and the normal of s'. This means:

$$\cos(\theta_-) = \cos(\theta) = 1 \tag{120}$$

Thus in this limit eq. 104 reduces to:

$$\lim_{|\vec{r}|\to\infty} \frac{\partial G}{\partial N} = \lim_{|\vec{r}|\to\infty} \left(\left(\frac{ik\exp(ikr)}{r} - \frac{\exp(ikr)}{r^2} \right) - \left(\frac{ik\exp(ikr_-)}{r_-} - \frac{\exp(ikr_-)}{{r_-}^2} \right) \right) \tag{121}$$

The substitution $\lim_{|\vec{r}|\to\infty} r_- = r$ can be made by remembering that the contribution from $(\vec{p_0} - \vec{p_{0-}})$ becomes negligible when $|\vec{r}|$ approaches ∞.

$$\lim_{|\vec{r}|\to\infty} \frac{\partial G}{\partial N} = \lim_{|\vec{r}|\to\infty} \left(\left(\frac{ik\exp(ikr)}{r} - \frac{\exp(ikr)}{r^2} \right) - \left(\frac{ik\exp(ikr_-)}{r} - \frac{\exp(ikr_-)}{r^2} \right) \right) \tag{122}$$

$$\updownarrow$$

$$\lim_{|\vec{r}|\to\infty} \frac{\partial G}{\partial N} = \lim_{|\vec{r}|\to\infty} G\left(ik - \frac{1}{r} \right) \tag{123}$$

$$\updownarrow$$

$$\lim_{|\vec{r}|\to\infty} \frac{\partial G}{\partial N} = ikG \tag{124}$$

Inserting in eq. 115:

$$\psi(P_0) = \frac{1}{4\pi} \iint_{s'} ds \left(-ik\psi G + G\frac{\partial \psi}{\partial N} \right) \tag{125}$$

$$\updownarrow$$

$$\psi(P_0) = \frac{1}{4\pi} \iint_{s'} dsG \left(-ik\psi + \frac{\partial \psi}{\partial N} \right) \tag{126}$$

Which in polar coordinates is:

$$\psi(P_0) = \frac{1}{4\pi} \iint_{\Omega} d\omega |\vec{r}|^2 G \left(-ik\psi + \frac{\partial \psi}{\partial N} \right) \tag{127}$$

Finally the Sommerfeld Radiation condition is[2]:

$$\lim_{|\vec{r}|\to\infty} |\vec{r}| \left(\frac{\partial \psi}{\partial N} - ik\psi \right) = 0 \tag{128}$$

The condition can be confirmed for a harmonic plane wave traveling along the wavevector $\left(\vec{r} \parallel \vec{k}\right)$. eq. 91 is differentiated along the normal of s' which always will be along the direction of travel for $|\vec{r}| \to \infty$:

$$\frac{\partial \psi}{\partial N} = \frac{\partial \psi}{\partial \vec{r}} = ikAe^{i\left(\vec{r}\cdot\vec{k}\pm\omega t\right)} = ik\psi \tag{129}$$

It can also be confirmed for a spherical wave originating within V.

The integral in eq. 115 is thus only non-zero over Σ. For P on Σ the distances r and r_- are identical since P_{0-} is P_0 mirrored in Σ which using eq. 103 means $G = 0$. Similarly the angles θ and θ_- are always mirrored around 90° or 270° which means $cos(\theta) = -cos(\theta_-)$. Thus:

$$\frac{\partial G}{\partial N} = \cos(\theta)\left(\frac{ik\exp(ikr)}{r} - \frac{\exp(ikr)}{r^2}\right) + \cos(\theta)\left(\frac{ik\exp(ikr)}{r} - \frac{\exp(ikr)}{r^2}\right) \tag{130}$$

$$\updownarrow$$

$$\frac{\partial G}{\partial N} = 2cos(\theta)\left(\frac{ik\exp(ikr)}{r} - \frac{\exp(ikr)}{r^2}\right) \tag{131}$$

It is possible to simplify further given that the wavelength is typically much smaller than the distances:

$$r >> \lambda \tag{132}$$

$$\downarrow$$

$$\frac{2\pi}{\lambda} = k >> \frac{1}{r} \tag{133}$$

eq. 131 becomes:

$$\frac{\partial G}{\partial N} = 2\cos(\theta)\frac{ik\exp(ikr)}{r} \tag{134}$$

Inserting into eq. 115 and remembering that $G(P) = 0$ for P on Σ:

$$\psi(P_0) = \frac{1}{4\pi}\iint_\Sigma ds\left(-2ik\psi(P)\cos(\theta)\frac{\exp(ikr)}{r}\right) \tag{135}$$

$$\updownarrow$$

$$\psi(P_0) = \frac{k}{2i\pi}\iint_\Sigma ds\left(\psi(P)\cos(\theta)\frac{\exp(ikr)}{r}\right) \tag{136}$$

$$\updownarrow$$

$$\psi(P_0) = \frac{1}{i\lambda}\iint_\Sigma ds\left(\psi(P)\cos(\theta)\frac{\exp(ikr)}{r}\right) \tag{137}$$

This is the first Rayleigh-Sommerfeld solution which mathematically shows Huygens-Fresnel Principle[2].

11.3 Paraxial approximation

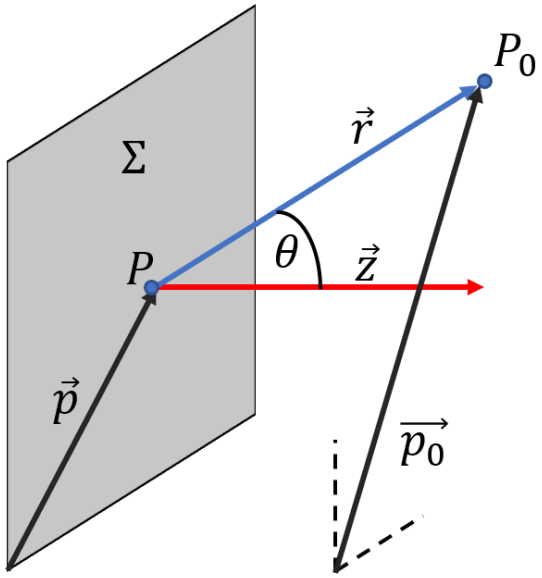

Figure 41: Illustration showing the different vectors. Not to scale since it is later assumed that $z >> |\vec{p_0} - \vec{p}|$

Here it is exploited that the distance along the direction of travel is usually much larger than the size of the sample and aperture. First, from trigonometry it is known that:

$$\cos(\theta) = \frac{z}{r} \tag{138}$$

This is substituted into eq. 137:

$$\psi(P_0) = \frac{1}{i\lambda} \iint_{\Sigma} ds \left(\psi(P) \frac{z \exp(ikr)}{r^2} \right) \tag{139}$$

The distance r can be expanded into the contributions from the Cartesian components where z is set to point opposite the normal of Σ and thus in the direction of the incoming wavevector. See figure 41.

$$r = \sqrt{z^2 + |\vec{p_0} - \vec{p}|^2} \tag{140}$$

It can in the denominator of eq. 139 be approximated that $r \approx z$ by assuming the distance z is much larger than $|\vec{p_0} - \vec{p}|$. This approximation can not be made for r in the exponential since k is

a large number a small change of r will make a non-negligible difference to the exponential. In this case r is further expanded to second order about its z-coordinate using the binomial expansion:

$$\sqrt{z^2+\left|\vec{p_0}-\vec{p}\right|^2} = z\sqrt{1+\left(\frac{\left|\vec{p_0}-\vec{p}\right|}{z}\right)^2} \approx z\left(1+\frac{1}{2}\left(\frac{\left|\vec{p_0}-\vec{p}\right|}{z}\right)^2\right) \tag{141}$$

These approximation are inserted into eq. 139 and z in the denominator is taken outside the integral since all points on Σ have equal distance z. To clarify it is here made explicit which variables depend on the position on the surface s:

$$\psi(P_0) = \frac{1}{iz\lambda}\iint_\Sigma ds\left(\psi(P(s))\exp\left(ikz\left(1+\frac{1}{2}\left(\frac{\left|\vec{p_0}-\vec{p(s)}\right|}{z}\right)^2\right)\right)\right) \tag{142}$$

$$\updownarrow$$

$$\psi(P_0) = \frac{\exp(ikz)}{iz\lambda}\iint_\Sigma ds\left(\psi(P(s))\exp\left(ik\frac{\left|\vec{p_0}-\vec{p(s)}\right|^2}{2z}\right)\right) \tag{143}$$

This is the Fresnel-Kirchhoff integral, also known as the Fresnel diffraction integral. It shows that the wavefunction at a position in V can be viewed as the sum of the contributions from an infinite number of Huygens point sources.

11.4 Rewriting the Fresnel-Kirchhoff integral using the Fourier transform

$\mathscr{F}$ is the two-dimensional Fourier transform:

$$\mathscr{F}(\psi(x,y)) = \iint \psi(x,y)\cdot\exp\left(-i\cdot 2\pi\cdot(x\cdot x'+y\cdot y')\right)dxdy \tag{144}$$

$$\mathscr{F}^{-1}(\psi(x',y')) = \iint \psi(x',y')\cdot\exp\left(i\cdot 2\pi\cdot(x'\cdot x+y'\cdot y)\right)dx'dy' \tag{145}$$

A convolution is defined as:

$$f(x,y)*g(x,y) = \iint f(t_x,t_y)g(x-t_x,y-t_y)dt_ydt_x \tag{146}$$

The convolution theorem states:

$$\mathscr{F}\left(f(x)*g(x)\right) = \mathscr{F}\left(f(x)\right)\mathscr{F}\left(g(x)\right) \tag{147}$$

Rewriting eq. 143 as a convolution with respect to $\vec{p_0}$:[4]

$$\psi(\vec{p_0}) = \frac{\exp(ikz)}{iz\lambda}\left(\psi_\Sigma(\vec{p_0}) * \exp\left(ik\frac{|\vec{p_0}|^2}{2z}\right)\right) \tag{148}$$

Turning the convolution into multiplication by taking the Fourier transform and using the convolution theorem[2]:

$$\mathscr{F}\left(\psi(\vec{p_0})\right) = \frac{\exp(ikz)}{iz\lambda}\mathscr{F}\left(\psi_\Sigma(\vec{p_0})\right)\mathscr{F}\left(\exp\left(ik\frac{|\vec{p_0}|^2}{2z}\right)\right) \tag{149}$$

The Fourier transform of the exponential can be treated like the Fourier transform of a bell-curve by extending the fraction by i:

$$\mathscr{F}\left(\exp\left(ik\frac{|\vec{p_0}|^2}{2z}\right)\right) = \mathscr{F}\left(\exp\left(-\pi\frac{|\vec{p_0}|^2}{iz\lambda}\right)\right) \tag{150}$$

Writing out the Fourier transform:

$$\mathscr{F}\left(\exp\left(ik\frac{|\vec{p_0}|^2}{2z}\right)\right) = \iint \exp\left(-\pi\frac{|\vec{p_0}|^2}{iz\lambda}\right)\cdot\exp\left(-i\cdot 2\pi\cdot\left(\vec{p_0}\cdot\vec{p'}\right)\right)d\vec{p_0} \tag{151}$$

$$\updownarrow$$

$$\mathscr{F}\left(\exp\left(ik\frac{|\vec{p_0}|^2}{2z}\right)\right) = \iint \exp\left(-\pi\left(\frac{|\vec{p_0}|^2}{iz\lambda} + i\cdot 2\cdot\left(\vec{p_0}\cdot\vec{p'}\right)\right)\right)d\vec{p_0} \tag{152}$$

Multiplying with $\exp\left(-\pi i^3 z\lambda\vec{p'}^2\right)$ in the integral and dividing it outside:

$$\mathscr{F}\left(\exp\left(ik\frac{|\vec{p_0}|^2}{2z}\right)\right) = \exp\left(\pi i^3 z\lambda\vec{p'}^2\right)\iint \exp\left(-\pi\left(\frac{|\vec{p_0}|^2}{iz\lambda} + i\cdot 2\cdot\left(\vec{p_0}\cdot\vec{p'}\right) + \vec{p'}^2 i^3 z\lambda\right)\right)d\vec{p_0} \tag{153}$$

Rewriting by reducing to the square of two terms:

$$\mathscr{F}\left(\exp\left(ik\frac{|\vec{p_0}|^2}{2z}\right)\right) = \exp\left(\pi i^3 z\lambda\vec{p'}^2\right)\iint \exp\left(-\pi\left(\frac{\vec{p_0}}{\sqrt{iz\lambda}} + \vec{p'}\sqrt{i^3 z\lambda}\right)^2\right)d\vec{p_0} \tag{154}$$

Doing integration by substitution:

$$\vec{u} = \frac{\vec{p_0}}{\sqrt{iz\lambda}} + \vec{p'}\sqrt{i^3 z\lambda} \tag{155}$$

Since $\vec{p'}$ lies in the xy-plane and the integral is infinite in x and y the translation by $\vec{p'}\sqrt{i^3 z\lambda}$ can be ignored:

$$d\vec{p_0} = \sqrt{iz\lambda}\,d\vec{u} \tag{156}$$

$$\mathscr{F}\left(\exp\left(ik\frac{|\vec{p_0}|^2}{2z}\right)\right) = \exp\left(\pi i^3 z\lambda \vec{p'}^2\right) iz\lambda \iint \exp\left(-\pi\left(u\right)^2\right) d\vec{u} \tag{157}$$

The two dimensional integral of a Gaussian function is:

$$\iint \exp\left(-a\left(x^2+y^2\right)\right) dxdy = \frac{\pi}{a} \tag{158}$$

Thus:

$$\iint \exp\left(-\pi\left(u\right)^2\right) d\vec{u} = 1 \tag{159}$$

And eq. 157 becomes:

$$\mathscr{F}\left(\exp\left(ik\frac{|\vec{p_0}|^2}{2z}\right)\right) = \exp\left(\pi i^3 z\lambda \vec{p'}^2\right) iz\lambda \tag{160}$$

Taking the inverse Fourier transform of eq. 149 after substituting:

$$\mathscr{F}\left(\psi(\vec{p_0})\right) = \mathscr{F}\left(\psi_\Sigma(\vec{p_0})\right) \exp\left(\pi i^3 z\lambda \vec{p'}^2 + ikz\right) \tag{161}$$

$$\updownarrow$$

$$\psi(\vec{p_0}) = \mathscr{F}^{-1}\left(\mathscr{F}\left(\psi_\Sigma(\vec{p_0})\right) \exp\left(\pi i^3 z\lambda \vec{p'}^2 + ikz\right)\right) \tag{162}$$

$$\updownarrow$$

$$\psi(\vec{p_0}) = \mathscr{F}^{-1}\left(\mathscr{F}\left(\psi_\Sigma(\vec{p_0})\right) \exp\left(-i2\pi^2 z k^{-1} \vec{p'}^2 + ikz\right)\right) \tag{163}$$

11.5 Aberration Space

In the above alternate version of the Fresnel-Kirchhoff integral the incoming wave is convoluted by a kernel describing the effects of the imaging system. By expanding the kernel using a Taylor series in Fourier space it is possible to describe the different contributions individually [5]:

$$\psi(\vec{p_0}, C_{mn}) = \mathscr{F}^{-1}\left(\mathscr{F}\left(\psi_\Sigma(\vec{p_0})\right) \exp\left(i4\pi^2 \sum_{m,n} C_{mn} x'^m y'^n + ikz\right)\right) | \{m,n\} \in \{0,1,2,...\} \tag{164}$$

$$C_{02} = C_{20} = -\frac{z}{2k} \tag{165}$$

$$\{C_{mn} | \{m,n\} \notin \{\{0,2\},\{2,0\}\}\} = 0 \tag{166}$$

For all further equations it is implicit that $\{m, n\} \in \{0, 1, 2, ...\}$.

The coefficients C_{mn} correspond to aberrations which characterize the imaging system, in this case every coefficient is zero except the two in eq. 165 representing defocus aberrations [5]. In general the coefficients can be written as the sum of a real and an imaginary part:

$$C \equiv C_{mn}^{(R)} + iC_{mn}^{(I)} \tag{167}$$

The real part preserves the norm of the wavefunction while the imaginary does not [5]. An equation describing the change in the wavefunction with repsect to a change in an aberration can be reached by differentiating eq. 164 with respect to a specific real or imaginary coefficient (m', n'):

$$\frac{\partial\psi(\vec{p_0})}{\partial C_{m'n'}^{(R)}} = \frac{\partial}{\partial C_{m'n'}^{(R)}}\left(\mathscr{F}^{-1}\left(\mathscr{F}\left(\psi_\Sigma(\vec{p_0})\right)\exp\left(i4\pi^2\sum_{m,n}C_{mn}x'^m y'^n + ikz\right)\right)\right) \tag{168}$$

$$\downarrow$$

$$\frac{\partial\psi(\vec{p_0})}{\partial C_{m'n'}^{(R)}} = \mathscr{F}^{-1}\left(\mathscr{F}\left(\psi_\Sigma(\vec{p_0})\right)\frac{\partial}{\partial C_{m'n'}^{(R)}}\exp\left(i4\pi^2\sum_{m,n}C_{mn}x'^m y'^n + ikz\right)\right) \tag{169}$$

$$\downarrow$$

$$\frac{\partial\psi(\vec{p_0})}{\partial C_{m'n'}^{(R)}} = \mathscr{F}^{-1}\left(\mathscr{F}\left(\psi_\Sigma(\vec{p_0})\right)i4\pi^2 x'^{m'}y'^{n'}\exp\left(i4\pi^2\sum_{m,n}C_{mn}x'^m y'^n + ikz\right)\right) \tag{170}$$

Setting:

$$U(x', y') = \mathscr{F}\left(\psi_\Sigma(\vec{p_0})\right)\exp\left(i4\pi^2\sum_{m,n}C_{mn}x'^m y'^n + ikz\right) \tag{171}$$

$$\frac{\partial\psi(\vec{p_0})}{\partial C_{m'n'}^{(R)}} = \mathscr{F}^{-1}\left(U(x', y')i4\pi^2 x'^{m'}y'^{n'}\right) \tag{172}$$

The same result can be achieved by using $\frac{i4\pi^2}{(i2\pi)^{n'+m'}}\frac{\partial^{m'}}{\partial x^{m'}}\frac{\partial^{n'}}{\partial y^{n'}}$:

$$\frac{i4\pi^2}{(i2\pi)^{n'+m'}}\frac{\partial^{m'}}{\partial x^{m'}}\frac{\partial^{n'}}{\partial y^{n'}}\psi(\vec{p_0}) = \frac{i4\pi^2}{(i2\pi)^{n'+m'}}\frac{\partial^{m'}}{\partial x^{m'}}\frac{\partial^{n'}}{\partial y^{n'}}\left(\mathscr{F}^{-1}U(x', y')\right) \tag{173}$$

$$\updownarrow$$

$$\frac{i4\pi^2}{(i2\pi)^{n'+m'}}\frac{\partial^{m'}}{\partial x^{m'}}\frac{\partial^{n'}}{\partial y^{n'}}\psi(\vec{p_0}) = \iint dx'dy'\left(U\left(x', y'\right)\frac{i4\pi^2}{(i2\pi)^{n'+m'}}\frac{\partial^{m'}}{\partial x^{m'}}\frac{\partial^{n'}}{\partial y^{n'}}\exp\left(i2\pi\left(x'x + y'y\right)\right)\right) \tag{174}$$

$$\updownarrow$$

$$\frac{i4\pi^2}{(i2\pi)^{n'+m'}}\frac{\partial^{m'}}{\partial x^{m'}}\frac{\partial^{n'}}{\partial y^{n'}}\psi(\vec{p_0}) = \iint dx'dy' \left(U\left(x',y'\right) i4\pi^2 x'^{m'} y'^{n'} \exp\left(i2\pi\left(x'x+y'y\right)\right)\right) \tag{175}$$

$$\updownarrow$$

$$\frac{i4\pi^2}{(i2\pi)^{n'+m'}}\frac{\partial^{m'}}{\partial x^{m'}}\frac{\partial^{n'}}{\partial y^{n'}}\psi(\vec{p_0}) = \mathscr{F}^{-1}\left(U(x',y') i4\pi^2 x'^{m'} y'^{n'}\right) \tag{176}$$

The result in eq. 172 and eq. 176 are equal, thus:

$$\frac{\partial}{\partial C^{(R)}_{m'n'}}\psi(\vec{p_0}) = \frac{i4\pi^2}{(i2\pi)^{n'+m'}}\frac{\partial^{m'}}{\partial x^{m'}}\frac{\partial^{n'}}{\partial y^{n'}}\psi(\vec{p_0}) \tag{177}$$

A similar derivation can be done for the imaginary part of the coefficient; the result is:

$$\frac{\partial}{\partial C^{(I)}_{m'n'}}\psi(\vec{p_0}) = -\frac{4\pi^2}{(i2\pi)^{n'+m'}}\frac{\partial^{m'}}{\partial x^{m'}}\frac{\partial^{n'}}{\partial y^{n'}}\psi(\vec{p_0}) \tag{178}$$

These partial differential equations describe the change of the wavefunction with respect to a change in one of the aberration coefficients. Note that these results differ slightly from the references since a different choice for the Fourier transform is used.

Following Paganin et al. the aberration coefficients are set to be function of a real variable τ:[5]

$$C_{mn}(\tau) = C^{(R)}_{mn}(\tau) + iC^{(I)}_{mn}(\tau) \tag{179}$$

Assuming the first derivative with respect to τ is finite:

$$\frac{\partial}{\partial\tau}\psi(\vec{p_0}, C(\tau)) = \sum_{m,n}\left(\frac{\partial\left(C^{(R)}_{mn}(\tau) + C^{(I)}_{mn}(\tau)\right)}{\partial\tau}\frac{\partial\psi(\vec{p_0}, C(\tau))}{\partial\left(C^{(R)}_{mn}(\tau) + C^{(I)}_{mn}(\tau)\right)}\right) \tag{180}$$

Using the chain rule with multiple intermediate functions this can be rewritten as:

$$\frac{\partial}{\partial\tau}\psi(\vec{p_0}, C(\tau)) = \sum_{m,n}\left(\frac{\partial C^{(R)}_{mn}(\tau)}{\partial\tau}\frac{\partial\psi(\vec{p_0}, C(\tau))}{\partial C^{(R)}_{mn}(\tau)} + \frac{\partial C^{(I)}_{mn}(\tau)}{\partial\tau}\frac{\partial\psi(\vec{p_0}, C(\tau))}{\partial C^{(I)}_{mn}(\tau)}\right) \tag{181}$$

Substituting the derivative with respect to the aberration coefficients for the results in eq. 177 and eq. 178:

$$\frac{\partial}{\partial\tau}\psi(\vec{p_0}, C(\tau)) = \mathscr{L}(\tau)\psi(\vec{p_0}, C(\tau)) \tag{182}$$

$$\mathscr{L} = \sum_{m,n}\frac{4\pi^2}{(i2\pi)^{n+m}}\left(i\frac{\partial C^{(R)}_{mn}(\tau)}{\partial\tau} - \frac{\partial C^{(I)}_{mn}(\tau)}{\partial\tau}\right)\frac{\partial}{\partial x^m}\frac{\partial}{\partial y^n} \tag{183}$$

11.6 Tilt aberration

With an equation describing the effects from tilt aberration separately it is possible to show how a combination of images at different tilt make it possible to determine the phase of the wavefunction. $C_{01}^{(I)}$ and $C_{10}^{(I)}$ represent incoherent tilt aberration. It is now assumed that only these aberration coefficients are a linear function of τ, which we then call tilt, and the remaining are set to zero:

$$\{C_{mn}^{(R)}\} = 0 \tag{184}$$

$$C_{01}^{(I)} = C_{10}^{(I)} = \gamma\tau \tag{185}$$

$$\{C_{mn}^{(I)} | \{m,n\} \notin \{\{0,1\},\{1,0\}\}\} = 0 \tag{186}$$

γ is a real unknown factor that doesn't depend on τ. Eq. 182 becomes:

$$\frac{\partial}{\partial\tau}\psi(\vec{p_0}, C(\tau)) = i2\pi\gamma\nabla_\perp\psi(\vec{p_0}, C(\tau)) \tag{187}$$

$$\nabla_\perp = \left(\frac{\partial}{\partial x} + \frac{\partial}{\partial y}\right) \tag{188}$$

The wavefunction is substituted for its exponential form,[6] which is known to be a solution from eq. 91. The exponential form is here defined as:

$$\psi = \sqrt{I}\exp(i\phi) \tag{189}$$

$$\psi^* = \sqrt{I}\exp(-i\phi) \tag{190}$$

$$\phi = \vec{p_0}\cdot\vec{k} \pm \omega t \tag{191}$$

Where the intensity I at different wavevectors $\vec{k}$ implicitly is a function of the incoming wavefunction $\psi_\Sigma(\vec{p})$ and the imaging system $C(\tau)$. Inserting ψ in eq. 187:

$$\frac{\partial}{\partial\tau}\left(\sqrt{I}\exp(i\phi)\right) = i2\pi\gamma\nabla_\perp\left(\sqrt{I}\exp(i\phi)\right) \tag{192}$$

$$\updownarrow$$

$$\frac{\partial\sqrt{I}}{\partial\tau}\exp\left(i\phi\right)+i\sqrt{I}\exp\left(i\phi\right)\frac{\partial\phi}{\partial\tau}=i2\pi\gamma\left(\frac{\partial\sqrt{I}}{\partial x}+\frac{\partial\sqrt{I}}{\partial y}+i\sqrt{I}\nabla_{\perp}\phi\right)\exp\left(i\phi\right) \tag{193}$$

Multiplying both sides of eq. 193 with ψ^* and reducing:

$$\frac{\partial\sqrt{I}}{\partial\tau}\sqrt{I}+iI\frac{\partial\phi}{\partial\tau}=i2\pi\gamma\left(\frac{\partial\sqrt{I}}{\partial x}\sqrt{I}+\frac{\partial\sqrt{I}}{\partial y}\sqrt{I}+iI\nabla_{\perp}\phi\right) \tag{194}$$

Equating the real parts since all variables are defined to be real:[6]

$$\frac{\partial\sqrt{I}}{\partial\tau}\sqrt{I}=-2\pi\gamma I\nabla_{\perp}\phi \tag{195}$$

Dividing by I by assuming $I>0$:

$$\frac{\partial\sqrt{I}}{\partial\tau}\frac{1}{\sqrt{I}}=-2\pi\gamma\nabla_{\perp}\phi \tag{196}$$

Differentiating left hand side using the chain rule:

$$\frac{\partial I}{\partial\tau}\frac{1}{2I}=-2\pi\gamma\nabla_{\perp}\phi \tag{197}$$

Making the following substitution and multiplying both sides by two:

$$\frac{\partial\log\left(I\right)}{\partial\tau}=\frac{\partial I}{\partial\tau}\frac{1}{I} \tag{198}$$

eq. 197 becomes:

$$\frac{\partial\log\left(I\right)}{\partial\tau}=-4\pi\gamma\nabla_{\perp}\phi \tag{199}$$

Using the finite difference approximation the differential phase can be calculated as a function of the intensity of two images at nearby tilt.[6] The assumption made is that the logarithm of the intensity is linear in tilt between the two images. Here the spatial dependence is made explicit and converted to 2 dimensions. Note that the negative sign means that τ_1 and τ_2 have been flipped in the denominator:

$$\nabla_{\perp}\phi\left(\vec{p_0},\frac{\vec{\tau_1}+\vec{\tau_2}}{2}\right)=\frac{\log\left(I(\vec{p_0},\vec{\tau_2})\right)-\log\left(I(\vec{p_0},\vec{\tau_1})\right)}{4\pi\gamma\left(\vec{\tau_1}-\vec{\tau_2}\right)} \tag{200}$$

$$\updownarrow$$

$$\nabla_{\perp}\phi\left(\vec{p_0},\frac{\vec{\tau_1}+\vec{\tau_2}}{2}\right)=\log\left(\frac{I(\vec{p_0},\vec{\tau_2})}{I(\vec{p_0},\vec{\tau_1})}\right)\frac{1}{4\pi\gamma\left(\vec{\tau_1}-\vec{\tau_2}\right)} \tag{201}$$

11.7 Appendix References

[1] D. M. Paganin, *Coherent X-ray optics*, Oxford University Press, 2006.

[2] J. W. Goodman, *Introduction to Fourier Optics*, W. H. Freeman, 1968.

[3] G. Kirchhoff, "Zur Theorie der Lichtstrahlen." *Annalen der Physik*, 1883 **254**(4), 663-695.

[4] M. Nazarathy and J. Shamir, "Fourier optics described by operator algebra." *Journal of the Optical Society of America*, 1980, **70**(2), 150-159.

[5] D. Paganin, T. Petersen and M. Beltran, "Propagation of fully-coherent and partially-coherent complex scalar fields in aberration space." *Phys. Rev. A*, 2018, **97**, 023835.

[6] M. Beltran and H. Simons, "Incoherent tilt aberration and its utility in imaging problems", 2018